Improving Micro Free Flow Electrophoresis Device Performance

A DISSERTATION
SUBMITTED TO THE FACULTY OF
UNIVERSITY OF MINNESOTA
BY

Nicholas William Frost

IN PARTIAL FULFILLMENT OF THE REQUIREMENTS
FOR THE DEGREE OF
DOCTOR OF PHILOSOPHY

Michael T. Bowser, Advisor

May 2014

Acknowledgements

My journey into, and through, graduate school in chemistry would not have been possible without a number of educators and supporters. It has been said that students often choose career paths based on the subjects taught by their favorite teachers, my career path has been no different. I would like to thank them now in somewhat chronologically fashion.

I would like to thank Matt Lubben, my high school chemistry teacher, for introducing me to the sciences and how interesting and exciting they can be. It was in his classroom that my passion for chemistry started and he was the reason I chose to major in chemistry at the undergraduate level. Thank you Matt.

I would like to thank my undergraduate advisor, Dr. Mike Ross, at St. John's University for opening up the world of analytical chemistry to me. His knowledge, humor, and passion for the subject quickly made analytical chemistry my favorite subject and it's no surprise that I have chosen to make a career out of it. Thank you Mike.

Next, I would like to thank my graduate advisor, Mike Bowser. Joining his research group was the best decision I could have made upon entering graduate school. His insight guided my graduate research while also providing me with the space I needed to grow as a researcher and an academic. I will forever be grateful for this opportunity. Thank you Mike.

I would like to thank all Bowser group members I've had the pleasure of knowing and working alongside of, especially Bryan Fonslow, Eric Castro, Ryan Turgeon, Meng Jing, Thane Taylor, Amy Hogerton and Matt Geiger. Our thoughtful discussions about research and life have been invaluable.

I would also like to thank the other University of Minnesota chemistry faculty members, especially Edgar Arriaga, Phil Buhlmann, and Pete Carr. Our conversations on various topics may have seemed minor at the time, but they helped shape my graduate career and my future. Thank you Edgar, Phil, and Pete.

I would like to thank the Nanofabrication Center staff, especially Paul Kimani and Tony Whipple, for their expertise. Without you, many of the fabrication questions and sticking points may have gone unresolved. Thank you Paul and Tony.

I would like to thank my parents, Bill and Dawn, for all they have done to get me to this stage in my life. Their support of my education and lifelong goals has allowed me to reach this point. I love you both.

And last but certainly not least, I would like to thank my wife, Emily. Her patience and unwavering support through this process has been amazing and I truly could not have done it without you. I love you.

Dedicated to my parents, Bill and Dawn Frost, and my wife, Emily Frost

For their never-ending support

Abstract

Micro free flow electrophoresis (μFFE) is a separation technique that continuously separates analyte streams as they travel through an electric field applied perpendicularly to the flow in a microfluidic device. The continuous nature of this separation technique makes it an ideal choice for a number of applications including long term continuous monitoring and as a second dimension separation technique in a two dimensional separation scheme. In order for μFFE devices to reach their full potential in these applications, improvements to the stability of separated analyte streams and zero dead volume connections to these devices must be addressed. This work will detail a simple, yet effective, way for mitigating the effects of electrolysis bubbles on analyte stream stability in μFFE devices by addition of surfactant or organic modifier to the electrolyte carrier buffer. The longest stable μFFE separation performed on our devices is shown to support the effectiveness of this approach. An approach for making zero dead volume connections to μFFE devices will also be detailed. The first two dimensional separation performed with a μFFE device as the second separation dimension is shown to support the effectiveness of this interface. Finally, the fabrication and operation of a microchip electrophoresis-micro free flow electrophoresis device for seamless integration of two separation dimensions is shown.

Table of Contents

List of Figures

List of Abbreviations

1D	One Dimensional
2D	Two Dimensional
µFFE	Micro Free Flow Electrophoresis
µFFIEF	Micro Free Flow Isoelectric Focusing
µFFMEKC	Micro Free Flow Micellar Electrokinetic Chromatography
µFFZE	Micro Free Flow Zone Electrophoresis
aSi	Amorphous Silicon
BSA	Bovine Serum Albumin
CAD	Computer Aided Design
CAPS	N-Cyclohexyl-3-Aminopropanesulfonic Acid
CCD	Charge Coupled Device
CGE	Capillary Gel Electrophoresis
CE	Capillary Electrophoresis
CMC	Critical Micelle Concentration
CV	Cyclic Voltammetry
CZE	Capillary Zone Electrophoresis
DAQ	Data Acquisition
DNA	Deoxyribonucleic Acid
EOF	Electroosmotic Flow
FFE	Free Flow Electrophoresis

FFIEF	Free Flow Isoelectric Focusing
FFITP	Free Flow Isotachophoresis
FFZE	Free Flow Zone Electrophoresis
FTIR	Fourier Transform Infrared
GABA	γ-Aminobutyric Acid
GC	Gas Chromatography
HEPES	4-(2-Hydroxyethyl)-1-Piperazineethanesulfonic Acid
HPLC	High Performance Liquid Chromatography
IEF	Isoelectric Focusing
ITP	Isotachophoresis
LC x LC	Two Dimensional Liquid Chromatography
LIF	Laser Induced Fluorescence
ME	Microchip Electrophoresis
MEKC	Micellar Electrokinetic Chromatography
MOS	Metal Oxide Semiconductor
MS	Mass Spectrometry
MSE	Module for Separated Electrolysis
MudPIT	Multidimensional Protein Identification Technology
NMR	Nuclear Magnetic Resonance
pI	Isoelectric Point
SCX	Strong Cation Exchange
SDS	Sodium Dodecyl Sulfate

SERS	Surface Enhanced Raman Scattering
PDMS	Poly(dimethylsiloxane)
PECVD	Plasma Enhanced Chemical Vapor Deposition
PLA	Poly(lactide)
PMMA	Poly(methyl methacrylate)
RP	Reversed Phase
RSD	Relative Standard Deviation
ZDV	Zero Dead Volume
ZE	Zone Electrophoresis

Chapter 1

Introduction

1.1 Introduction to Microfluidic Separations

The field of microfluidics involves the manipulation of small volumes of fluid (μL to aL) contained in channels with dimensions of tens to hundreds of microns (micrometers).[1] Microfluidics in the field of chemical analysis offers many advantages to "benchtop" methods including smaller sample volume requirements, lower reagent consumption, lower cost, and shorter analysis times. The majority of reports involving microfluidic-based chemical separations utilize electrophoretic methods. The following section gives a brief history of chemical separations (primarily electrophoretic separations) in capillary format and, ultimately, their transition to microfluidic platforms.

1.1.1 Chemical Separations in Capillary Format

In a patent filed in 1981, the work of Bente III, Zerenner, and Dandeneau of the Hewlett-Packard Company® in which fused silica capillaries were developed and utilized in gas chromatography was detailed.[2] The use of fused silica capillaries for high-resolution gas chromatography was also detailed in the literature a few years prior by the same (and additional) authors.[3,4] The use of these fused silica capillaries in gas chromatography revolutionized the field and changed the future of column technologies. The majority of commercially available gas chromatography columns to date are still fused silica based. Gas chromatography in narrow bore open tubular capillary columns offers a number of advantages including increased separation efficiency (narrower peaks), faster

analysis times, and higher sensitivity. The use of narrow inner diameter packed fused silica capillary columns in liquid chromatography has also had an impact on separation efficiency and detection sensitivity in the field. Reports of capillary liquid chromatography in the literature have grown tremendously in the last two decades, including analyses of nucleic acids,[5,6] peptides,[7-10] and purines.[11]

The fused silica capillary had a profound effect on electrophoresis as a viable high-resolution separation technique. Traditional slab electrophoresis has been used for many decades as a means of separating components of biological samples (i.e., proteins) and is still the most widely used separation tool in biology and biochemistry.[12] Unfortunately, electrophoretic separations performed in this manner are often slow, offer limited quantitative information, and are labor intensive. The slow nature of slab-based electrophoresis is a product of the low applied voltages often used due to possible Joule heating. This is where fused silica capillaries made their mark in the field of electrophoresis. Fused silica capillaries have small inner diameters (generally tens of microns) and, in practice, often have lengths on the order of tens of centimeters. This small cross sectional area and long length creates an extremely high resistance to current flow. Or in other words, large potentials can be applied across a fused silica capillary with minimal current, limiting Joule heating and its effects on separation efficiency. Since longitudinal diffusion is generally the main source of band broadening in capillary electrophoresis, faster separations are essential to increasing separation performance. In order to perform fast separations, high

electric field strengths must be attainable and separations in fused silica capillaries provide this advantage. Numerous efficient separations of a variety of analytes have been reported using electrophoresis in fused silica capillaries and are detailed in many reviews.[13-15]

The introduction of capillary-based separations in gas chromatography, liquid chromatography, and electrophoresis clearly had a significant impact on the separation efficiency of these techniques. The push towards microfluidic based separations ultimately stemmed from this increased separation efficiency displayed in capillary format.

1.1.2 Chemical Separations on Microfluidic Platforms

The first report of a miniaturized chemical separation technique on a microfluidic platform was a gas chromatography-based air analyzer fabricated in silicon in 1979.[16] Microfluidic gas chromatography separations have not been widely reported since, for a variety of reasons, and will not be discussed further. Manz, Graber, and Widmer first reported the benefits of miniaturized total chemical analysis systems, with an emphasis on separations, in 1990.[17] Manz *et. al.* followed this report with the first documented open tubular liquid chromatography microchip fabricated in silicon.[18] Microchip liquid chromatography has found wider use than its gas chromatography counterpart but, again, is not the focus of this work and will not be discussed further. Microchip electrophoresis devices followed a few years later beginning in 1992.[19-

[22] Since these first reports, the field of microfluidic-based electrophoretic separations has exploded over the past twenty plus years as evidenced by the over 3,500 articles published since 1992 on the topic. The benefits of small diameter channels, short channel lengths, and electroosmotic flow (EOF) on separation efficiency and the relative ease with which liquids can be controlled electrokinetically have contributed to the large of number of electrophoretic-based microchip devices over pressure-driven, chromatography-based devices. These devices have been used in various modes, including zone electrophoresis (ZE),[23,24] micellar electrokinetic chromatography (MEKC),[25] sieving electrophoresis,[26] isotachophoresis (ITP),[27] and isoelectric focusing (IEF),[28,29] for a variety of analytes including DNA,[30] peptides,[31] proteins,[32,33] biogenic amines,[34] drug metabolites in urine,[35] and mitochondria.[36] The principles of some of the electrophoretic separation modes mentioned are discussed later in this work (Section 1.5.4.).

It should also be mentioned that commercially available products implementing lab-on-a-chip separation technologies are currently on the market including liquid chromatography-based devices (i.e., Agilent's 1260 Infinity HPLC-Chip and Eksigent's cHiPLC®) and electrophoresis-based devices (i.e., Agilent's DNA 1000/7500 LabChip® and Shimadzu's MCE®-202 MultiNA).

1.2 Micro Free Flow Electrophoresis (μFFE)

Many microfluidic systems for chemical analysis take inspiration from previously developed "macro" analytical techniques, much like the techniques discussed above which have been successfully implemented on microfluidic platforms. The miniaturization of free flow electrophoresis onto a microfluidic platform has followed a similar path.

1.2.1 Free Flow Electrophoresis (FFE)

Free flow electrophoresis (FFE) was initially introduced by Barrolier in 1958,[37] and later by Hannig in 1961,[38] as a means of continuously separating biopolymers (proteins, DNA, *etc.*). In FFE, a sample stream of analytes is separated in a pressure-driven hydrodynamic flow of electrolyte buffer by applying an electric field perpendicular to the overall electrolyte buffer flow (Figure 1.1). The application of an electric field perpendicular to the direction of fluid flow gives rise to a separation in space, not time, allowing for continuous application and separation of sample. By the late 1980's and early 90's, several studies showed the usefulness of FFE as a preparative technique in analysis of biological samples such as protein purification by free flow zone electrophoresis (FFZE),[39] free flow isotachophoresis (FFITP),[40,41] and free flow isoelectric focusing (FFIEF),[42] phospholipid purification by FFZE,[43,44] and separation of cell populations by FFZE.[45,46] The first mention of FFE in an analytical context was from Hannig in 1982,[47] but the techniques described suffered from poor

resolution due to excessive Joule heating, just as in preparative FFE.[48,49] The available materials and fabrication methods limited FFE instruments (devices) to relatively large dimensions and volumes, and therefore low surface area-to-volume ratios leading to poor heat dissipation. Poor heat dissipation limits the potential that can be applied to 60-90 V/cm.[49,50] The development of a more efficient FFE device would require significant miniaturization to allow for the application of a moderate electric field without causing substantial Joule heating within the separation space.

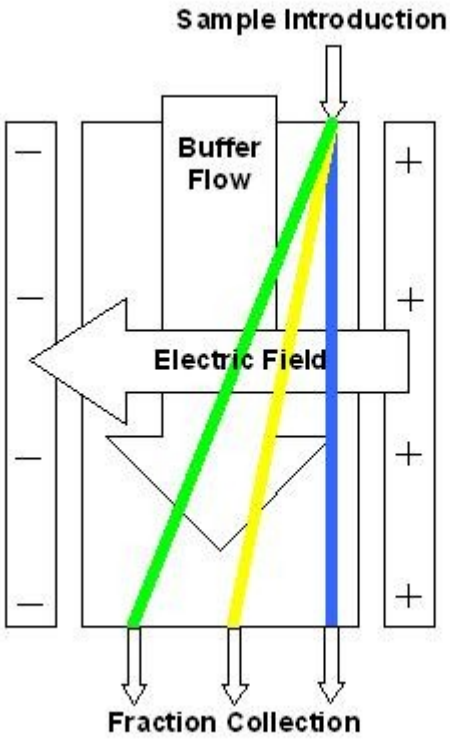

Figure 1.1. General principal of separation in FFE. Analyte streams are carried through the device via pressure-driven flow and deflected laterally in an electric field based on their total mobilities.

1.2.2 Progression of Micro Free Flow Electrophoresis (μFFE)

The first truly miniaturized μFFE device was reported by Raymond *et. al.* in 1994,[51] and later elaborated on in 1996,[52] involving micromachined channel systems in silicon. Raymond *et. al.* were able to show that the smaller separation volumes (25 μL as compared to >50 mL in large scale FFE devices) allowed for better heat dissipation and essentially no contribution to band broadening from Joule heating, while maintaining comparable resolution (~8 bands/cm) to commercially available FFE systems (~10 bands/cm).[51,52] The main drawback, however, of the original silicon μFFE device described by Raymond *et. al.* was the relatively low electric field strengths (~50 V/cm) that could be applied due to the low electrical breakdown voltage of silicon.

Equation 1.1[53] shows the relationship between migration distance of an analyte from its original position, electric field strength across the separation space, and residence time in the electric field,

$$d = \mu E t \quad (1.1)$$

where d is the deflection distance of an analyte (cm), μ is the mobility of the analyte (cm^2/V sec), E is the electric field strength across the separation space (V/cm) and t is the residence time in the electric field (sec). Resolution of an analyte pair in μFFE arises from a difference in deflection distance as shown in Equation 1.2.

$$\Delta d = d_2 - d_1 = \mu_2 Et - \mu_1 Et = \Delta\mu Et \quad (1.2)$$

As the strength of the electric field increases, the residence time within the separation space can be decreased proportionally, by increasing the linear flow velocity of the electrolyte buffer, without a loss in migration distance of a particular analyte. In other words, the overall residence time can be made considerably shorter at higher electric field strengths. It should be noted, however, that adjusting the electric field strength, linear flow velocity of the electrolyte buffer, and analyte migration distance can have drastic effects on sample resolution. Equation 1.2 above clearly shows that high electric field strengths can be advantageous in separating analytes with similar mobilities. In order to achieve higher electric field strengths, materials other than silicon would have to be investigated.

Materials commonly used in microfluidic device fabrication have also been used to make μFFE devices including glass[54-60], poly(dimethylsiloxane) (PDMS)[61-64], poly(methyl methacrylate) (PMMA)[65], and biaxially-oriented polyethylene terephthalate (Mylar™).[66] These materials offer a number of advantages over silicon including allowing higher applied voltages, lower materials cost, and optical transparency.

Fabrication in materials such as glass and PDMS has improved the performance of μFFE devices in terms of allowing higher electric field strengths. A thorough understanding of band broadening processes in μFFE is essential to

improving device performance even further. The variance of an analyte band in μFFE ($\sigma^2_{\mu FFE}$) can be expressed as the sum of all the contributing factors to broadening in the system,

$$\sigma^2_{\mu\mathrm{FFE}} = \sigma^2_{\mathrm{INJ}} + \sigma^2_{\mathrm{D}} + \sigma^2_{\mathrm{HD}} + \sigma^2_{\mathrm{EMD}} \qquad (1.3)$$

where σ^2_{INJ} is the broadening due to injection, σ^2_{D} is the diffusional broadening contribution, σ^2_{HD} is the hydrodynamic broadening contribution, and σ^2_{EMD} is the electromigration dispersion contribution.[67-69] The injection variance can be expressed by Equation 1.4,[70]

$$\sigma^2_{\mathrm{INJ}} = \frac{w^2_{INJ}}{12} \qquad (1.4)$$

where w^2_{INJ} is the width of the injected analyte band. Equation 1.4 shows that decreasing the width of the injected analyte band, decreases the contribution of injection broadening to the overall sample variance. In this instance, the width of the injected sample band will be dependent on hydrodynamic focusing upon transfer to the μFFE device. Hydrodynamic focusing occurs when neighboring laminar flow streams are flowing at higher linear velocities than the incoming sample stream.[54] In other words, the width of the incoming sample stream can be controlled by manipulating the linear velocity of the carrier buffer in the separation space, relative to the linear velocity of the incoming sample stream.

Band broadening due to analyte diffusion (in the space domain) can be expressed by Equation 1.5,[58]

$$\sigma_D^2 = 2Dt = \frac{2DL}{\nu} \qquad (1.5)$$

where D is the diffusion coefficient of the analyte, t is the residence time in the separation space, L is the length of the separation space (from sample inlet to detection), and ν is the linear flow velocity of the electrolyte buffer. It is clear that shorter residence times, or higher linear flow velocities, will minimize the contribution of analyte diffusion to the overall variance.

Hydrodynamic broadening in μFFE separations is a result of the pressure-driven parabolic flow profile of the electrolyte buffer in the μFFE chip. Fonslow has described hydrodynamic band broadening in detail.[57] Equation 1.6,

$$\sigma_{HD}^2 = \frac{h^2 d^2 \nu}{105DL} \qquad (1.6)$$

shows the dependence of the variance due to hydrodynamic broadening on the height of the separation channel, h, the migration distance of the analyte, d, the linear flow velocity of the electrolyte buffer, ν, the diffusion coefficient of the analyte, D, and the length of the separation space, L. Analytes with large diffusion coefficients will exhibit a smaller contribution to hydrodynamic broadening because they will be able to move more quickly between all linear velocities of the parabolic flow profile. Similarly, small separation channel heights, as is the case in our μFFE devices, drastically reduce hydrodynamic

broadening because analytes have a shorter distance to diffuse to reach all linear velocities of the parabolic flow profile. Increasing the linear velocity of the electrolyte buffer increases the contribution to hydrodynamic broadening by elongating the parabolic flow profile causing a wider range of residence times within the separation channel.

Electromigration dispersion arises in μFFE when the buffer composition over which the electric field is applied is not constant, or in other words, there are areas of differing conductivity within the separation channel. As bands migrate out of a flow stream of high conductivity into a flow stream of lower conductivity, broadening can occur due to the different speeds at which analytes travel in the different buffer compositions. Band broadening contributions from electromigration dispersion are usually not significant in μFFE separations since the sample buffer composition can be made similar to the carrier electrolyte buffer composition used to mobilize analytes through the chip. However, since one of the goals of this work is to perform two dimensional separations, the sample buffer composition is going to depend on the nature of the first dimension separation and electromigration dispersion may contribute significantly to the overall band broadening during the μFFE separation. Electromigration dispersion has been discussed in detail in the literature.[71-73]

Equations 1.4, 1.5, and 1.6 can be substituted into Equation 1.3 to describe the total variance of an analyte band in μFFE separations, Equation 1.7.[57]

$$\sigma^2_{\mu FFE} = \frac{w^2_{inj}}{12} + \frac{2DL}{\nu} + \frac{h^2 d^2 \nu}{105DL} + \sigma^2_{EMD} \qquad (1.7)$$

It is clear from Equation 1.7 that there is considerable interplay between linear flow velocity of the electrolyte buffer and analyte migration distance, which is a function of electric field strength and linear flow velocity (Equation 1.1), on the overall variance of an analyte band. Fonslow[58] took it one step further, assuming no contribution from electromigration dispersion, and described an equation that yields the optimum linear velocity to minimize band broadening if the analyte migration distance is known (Equation 1.8).

$$\nu_{opt} = \frac{\sqrt{210}DL}{hd} \qquad (1.8)$$

The ability to achieve high electric field strengths and a thorough understanding of broadening processes in μFFE is essential to maximizing device performance. However, two areas of improvement remain for μFFE devices to reach their true potential. Maintaining stability of separated analyte streams in μFFE devices has proven problematic and has hindered their long term use and will be addressed in Chapter 1, Section 3. The use of μFFE devices as both long term continuous monitoring devices and second dimension separation techniques in two dimensional separation schemes requires not only long term analyte stream stability, but also zero dead volume (ZDV) connections between incoming sample streams and the μFFE devices. If the goal is to monitor concentration changes over time (continuous monitoring), remixing of the

incoming sample stream upon transfer to the μFFE device will be quite detrimental. If the goal is to perform two dimensional separations, remixing of the first dimension sample stream upon transfer to the μFFE device will cause a loss of sample resolution from the first dimension. The applications discussed in detail later will require ZDV connections to maximize device performance. Zero dead volume connections to the μFFE devices will be addressed in Chapter 1, Section 4.

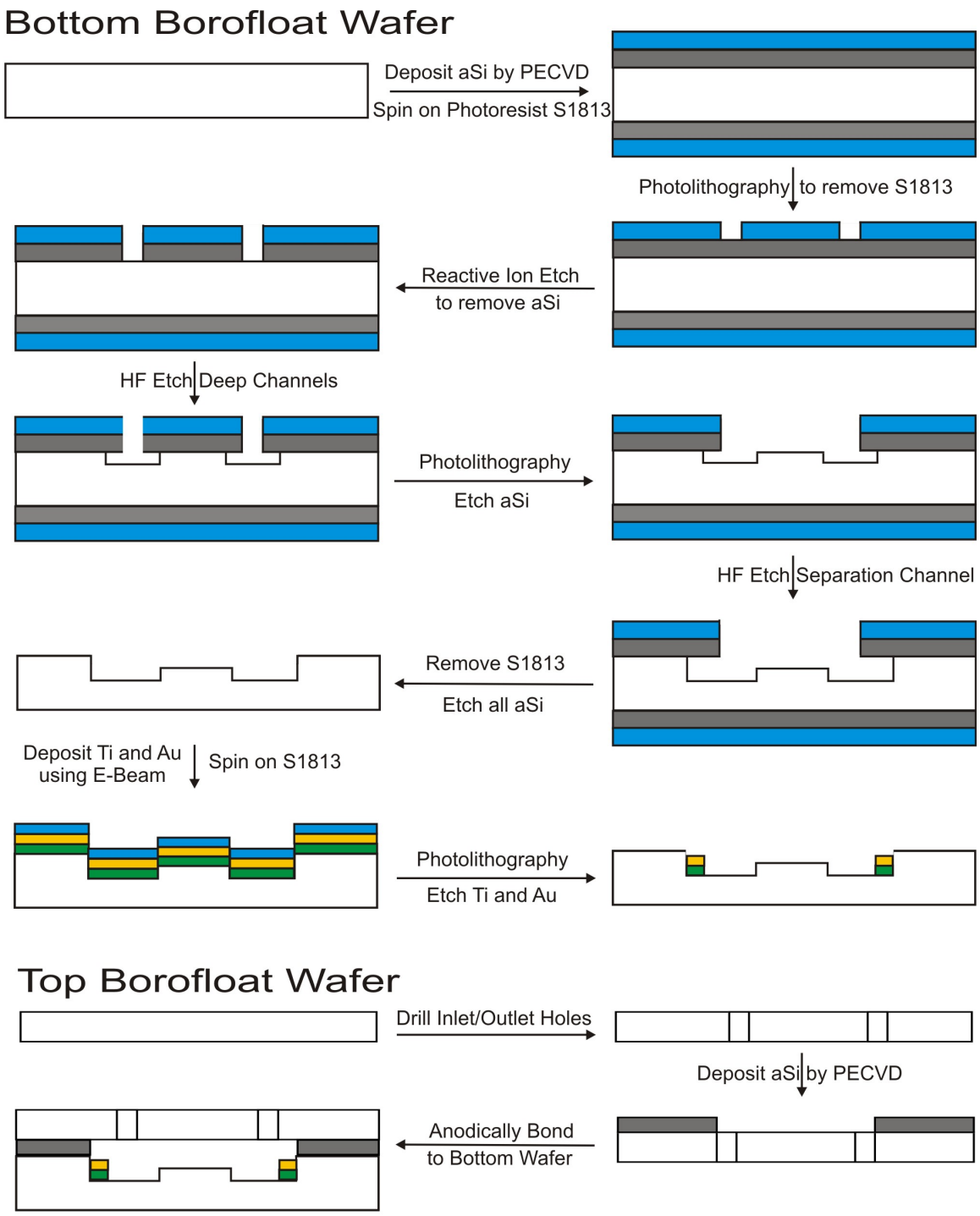

Figure 1.2. General fabrication scheme of an all glass µFFE device. Borosilicate glass (white), amorphous silicon (grey), positive photoresist (blue), titanium (green), gold (yellow).

1.2.3 Current µFFE Device Fabrication and Detection Scheme

All device fabrication described in this work follows a general process as outlined in Figure 1.2. Borosilicate glass wafers are masked with amorphous silicon through a plasma enhanced chemical vapor deposition (PECVD) process. Standard photolithography procedures are then used to define features to be etched in the glass. Wet etching techniques involving concentrated HF (49%) are then used to isotropically etch the borosilicate glass wafers. This wet etching process can be repeated a number of times to define regions of differing depth. Electrodes are fashioned out of titanium and gold layers deposited on the glass

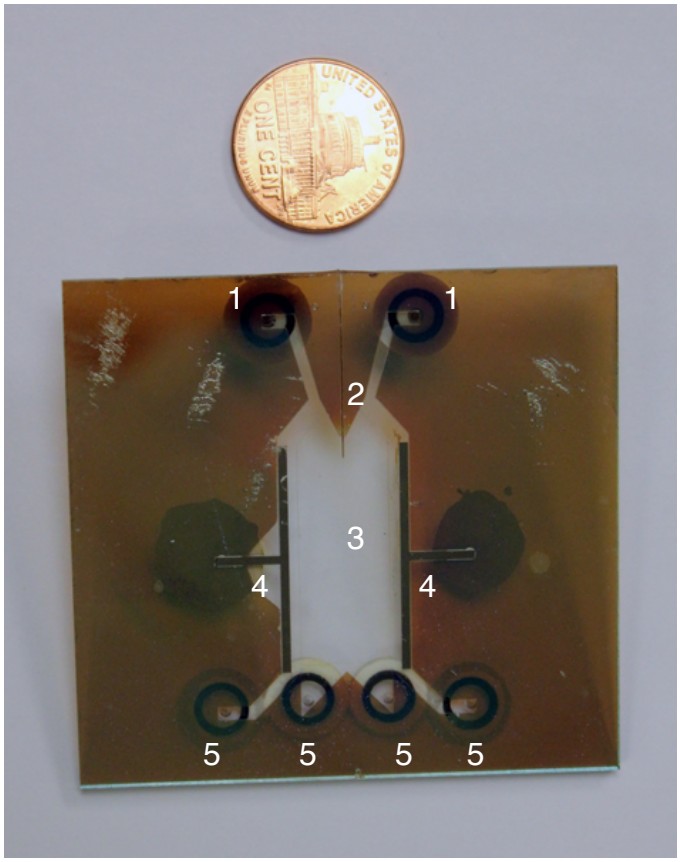

Figure 1.3. An example of a µFFE device used in Chapter 3 of this work. Buffer inlets (1), capillary insertion channel (2), separation chamber (3), electrodes (4), buffer outlets (5).

surface by electron beam evaporation followed by photolithography and wet etching to remove unwanted metal. A second borosilicate glass wafer is then pre-drilled with access holes and anodically bonded to the featured wafer with a thin layer of amorphous silicon between the glass substrates. An example of a completed device is shown below in Figure 1.3. A more detailed description of this fabrication process can be found in a number of group publications.[59,74,75]

Adequate detection schemes for microfluidic-based separation techniques are inherently a challenge due to short optical pathlengths and small sample volumes (and thus small sample mass). A number of detection schemes have been reported on various microfluidic lab-on-a-chip devices including amperometric,[76,77] conductivity,[78,79] cyclic voltammetry (CV),[80] fourier transform infrared (FTIR) spectroscopy,[81] surface enhanced Raman scattering (SERS),[82,83] fluorescence,[57-59] and even nuclear magnetic resonance (NMR) spectroscopy.[84,85] Several reviews have been published on this topic.[86,87]

Micro free flow electrophoresis requires a somewhat unique detection scheme in that detection must be performed in space, or over a given detection area. Many of the detection schemes commonly used in microfluidic lab-on-a-chip devices, such as the ones listed above, are known as point detection schemes. Point detectors involve detection as analyte moves past some fixed point in the separation scheme and are ideally suited for separations in time. In order for a point detection scheme to be implemented with a μFFE device, a mechanism allowing the device to be moved spatially must be utilized to detect

analyte over the width of the separation region. This type of detection scheme has been reported with μFFE devices,[51,52,65] but is not an ideal choice since the entire separation region cannot be monitored at once and requires precise control of the spatial movement of the device.

The detection scheme used in this work utilizes laser-induced fluorescence (LIF) with a charge-coupled device (CCD) camera to image over the entire width of the separation channel. The detection scheme is shown in Figure 1.4 below. Briefly, the 488 nm beam from an argon ion laser is expanded into a line and directed across the entire width of the separation space. A CCD camera attached to an optical microscope then captures fluorescent photons emitted by analyte molecules. A charge-coupled device is a two dimensional array of metal-oxide-semiconductor (MOS) capacitors which convert light intensity over an imaging space to a measurable electric current.

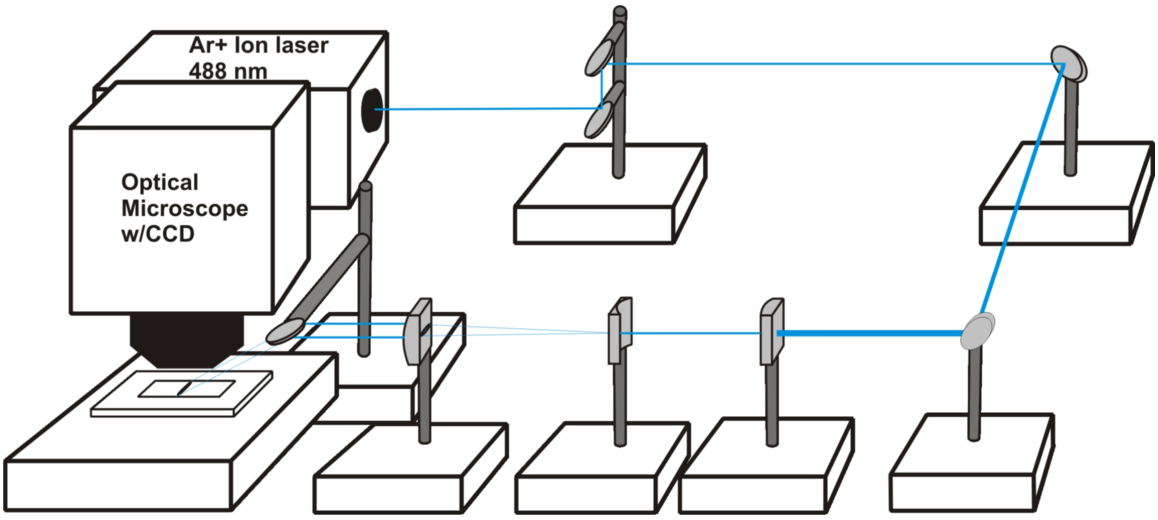

Figure 1.4. The μFFE detection scheme used in this work. The 488 nm beam of an argon ion laser is expanded into a line and directed across the separation space. An optical microscope with a CCD camera captures photons emitted from fluorescing species passing the detection zone.

1.3 Improving Analyte Stream Stability in µFFE Devices

Heat dissipation has not proven to be the limiting factor in the practical implementation of µFFE devices. Instead, the formation of bubbles at the electrode surface due to electrolysis has proven to be the most difficult issue. These bubbles disrupt the flow pattern and electric field in the device, giving rise to unpredictable analyte flow paths.[74] Devices fabricated which do not incorporate design aspects to mediate the effect of electrolysis bubbles are limited to very low applied voltages. For example, Macounova *et al.*[66,88] and Lu *et al.*[89] have recently reported such devices in which the applied voltage could not exceed 3 V before interference from electrolysis bubbles occurred.

Numerous design features aimed at controlling or removing electrolysis bubbles have been reported. Many early µFFE devices included arrays of microchannels fashioned to act as "membrane" barriers isolating the electrodes from the separation space,[51,52,58,61,62] which were meant to mimic the ion-exchange membranes, employed in conventional FFE devices. While these designs effectively prevented electrolysis bubbles from entering the separation space, the reduced cross sectional area of the membrane channels caused the majority of the applied potential to be experienced in the side channels, not the separation channel.[62,58] Photopolymerized acrylamide membranes have recently been incorporated into µFFE devices. Kohlheyer *et al.*[54,55] describe devices in which acrylamide membranes were used to isolate open electrode reservoirs

from the separation space to enable ventilation of gas bubbles. Electrolysis bubbles did not enter the separation space and voltage efficiencies of 40-60% were reported using these devices. A similar result was achieved by de Jesus *et al.*[90] using acrylamide membranes in side reservoirs and a complex module for separated electrolysis (MSE). An MSE acts to separate the electrodes from the separation space by containing them in an electrolyte-filled syringe connected to side reservoirs via polyethylene tubing. The authors reported continuous operation with an electric field of 192 V cm^{-1} in the separation channel for 3 hours without disturbances from electrolysis bubbles. Isolation of the electrodes using multiple depth designs has proven to be one of the simplest methods for decreasing electrolysis bubble interference while maintaining high voltage efficiencies. Fonslow *et al.* introduced a multiple depth design in which the electrode channels were four times deeper than the separation chamber resulting in a linear flow velocity over the electrodes that was 16 times greater than that in the separation channel, which effectively washed away electrolysis bubbles without interfering with the separation.[59],[57] Kobayashi *et al.*[91] have also reported a multiple depth design in which the electrodes are isolated by shallow side banks running along the edge of the separation space.

While much effort has been made to design devices that are better equipped to handle the formation of electrolysis bubbles while keeping the voltage efficiency high, there has been less success removing or controlling electrolysis bubbles through buffer modification. Kohlheyer *et al.*[56] have reported

bubble-free operation of a μFFE device by adding a redox couple, quinhydrone, to the flow streams near the electrodes. The oxidation and reduction of the redox couple generates the electrical current without formation of electrolysis bubbles. While this approach was successful in improving the resolution of separated analyte streams, local pH changes near the electrodes due to the oxidation and reduction of the redox species caused a pH gradient to form across the separation chamber.

In this work, buffer modification by addition of surfactant or organic solvent is reported as a means of improving analyte stream stability by mitigating the effects of electrolysis bubbles in the separation space (Chapter 2).

1.4 Zero Dead Volume Connections to μFFE Devices

Two applications of μFFE devices that have yet to be fully realized are long term continuous monitoring and two dimensional separations with a μFFE device as the second dimension. Being able to make zero dead volume (ZDV) connections from μFFE devices to the outside world is essential in both of the applications mentioned. In long term continuous monitoring, concentration changes are monitored continuously as a function of time from an incoming sample stream. If the incoming sample stream encounters regions of substantial dead volume, mixing of the stream can occur and potential concentration dynamics can be blurred or lost all together. In two dimensional separations a

similar concern exists. If the sample stream from the first dimension encounters a region of substantial dead volume during the transfer to the second dimension, remixing of the sample stream can occur causing a loss in sample resolution gained in the first dimension. It is clear that zero dead volume connections must be implemented for both long term continuous monitoring and two dimensional separation applications to reach their full potential.

There is surprisingly little in the literature pertaining to zero dead volume connections with microfluidic devices, especially considering the implications discussed above. Commercially available products exist (Nanoports™ by IDEX Health and Science being the most popular) for making fluidic connections to microfluidic devices. Despite claims of zero (or minimal) dead volume, these products do not provide the necessary connections needed in this work as evidenced in numerous experiments. The need for standard connections in microfluidics to make these types of connections has been recently reviewed.[92]

The most often cited work for minimizing dead volume was performed by Bings *et. al.* in which fused silica capillary connections were made to microfluidic channels by drilling into the edge of the device with small diameter drill bits.[93] Briefly, standard pointed tip drill bits as small as 200 µm in diameter were used to drill a hole into the edge of the device that is lined up with the microfluidic channel. Then, a flat bottom drill bit of the same diameter was used to flatten the bottom of the hole to ideally remove any dead volume in the connection (see Figure 1.5). The efficacy of this capillary-device interface was tested by looking

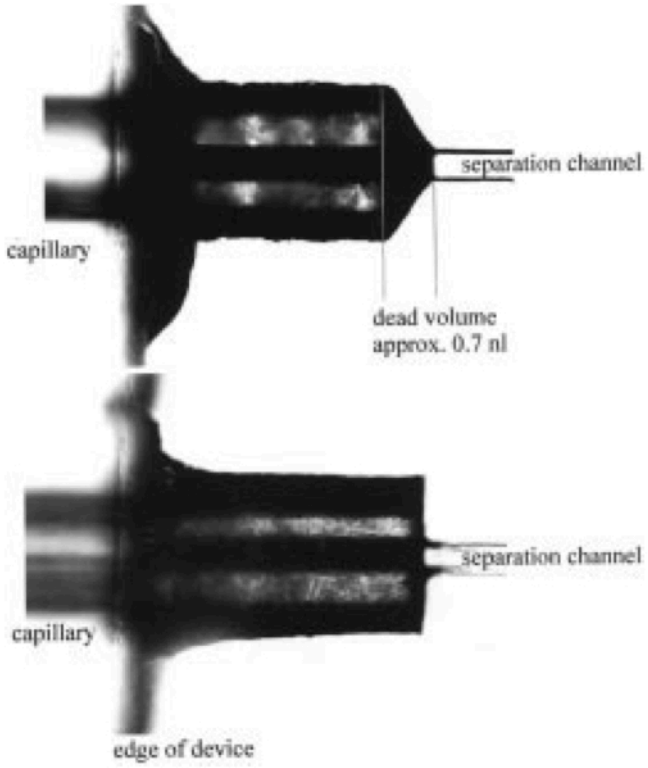

Figure 1.5. Fused silica capillary connections to a microfluidic channel. The procedure of making these connections is detailed in ref. 93. Image adapted from ref. 93.

at the number of theoretical plates of analyte peaks immediately before the interface and immediately after the interface. The authors report that, on average, ~98% of the predicted theoretical plates remained after travel through the interface indicating minimal dead volume. Unfortunately, this interface is not easily adapted to μFFE devices for two main reasons. First, the capillary connection to be made is with an open separation space, not a microfluidic channel, making it difficult to drill into the separation space without glass fragments getting lodged into the space. Second, the geometry of the μFFE

devices would require holes being drilled over several centimeters to reach the separation space, making alignment difficult.

The need for new strategies to make zero dead volume connections to μFFE devices is evident. Several strategies for making capillary connections to μFFE devices will be discussed in detail in Chapter 3.

1.5 Two Dimensional Separations

1.5.1 The Need For High Peak Capacity Separation Techniques

With the recent explosion in the number of "omic" studies worldwide (genomics, proteomics, metabolomics, *etc.*), the development of separation techniques with enough resolving power to analyze complex sample mixtures containing hundreds to tens of thousands of constituents, at a wide range of concentrations, has become increasingly important. For example, it has been shown that even a single-celled organism, such as *E. coli*, can express over 4,200 proteins.[94] Also, metabolomic studies, which are the analyses of low molecular weight (<1,000 Da) metabolites in cells, tissues, or biofluids,[95] have shown the presence of over 3,000 metabolites in a liver tissue sample of *Limanda limanda*, a marine flatfish.[96] It is clear that separation techniques capable of resolving a large number of sample components are necessary in these fields.

Interestingly, an often-overlooked advantage of large peak capacity separation techniques is their usefulness in separating relatively simple sample mixtures. Often, considerable time is spent in optimizing a separation technique for a particular sample to maximize the number of separated components. Work by Martin, Herman, and Guiochon describing the probability all sample components are resolved, $P_{m,n}(m)$, for a given peak capacity, n, and a given number of components in the sample mixture, m, is given in Equation 1.9.[97]

$$P_{m,n}(m) = \left(1 - \frac{m-1}{n-1}\right)^{m-2} \qquad (1.9)$$

The impact of this equation can be seen in Figure 1.9 where the probability all sample components are resolved, $P_{m,n}(m)$, is plotted versus number of sample components, m, for two given peak capacities (100 and 2000).

For a relatively simple sample mixture of 20 components, there is only a ~2% chance that all 20 components will be resolved using a separation technique with a peak capacity of 100 and no previous optimization. This assumes that peak positions are randomly distributed in the separation space and peaks widths of all components are the same. In this scenario, the researcher would have to spend considerable time optimizing this separation in hopes of ultimately separating all 20 components. Using a separation technique with a peak capacity of 2000, the probability of resolving all 20 sample components without separation optimization is ~84%. The power of high peak capacity separations in the analysis of simple sample mixtures is obvious. It is

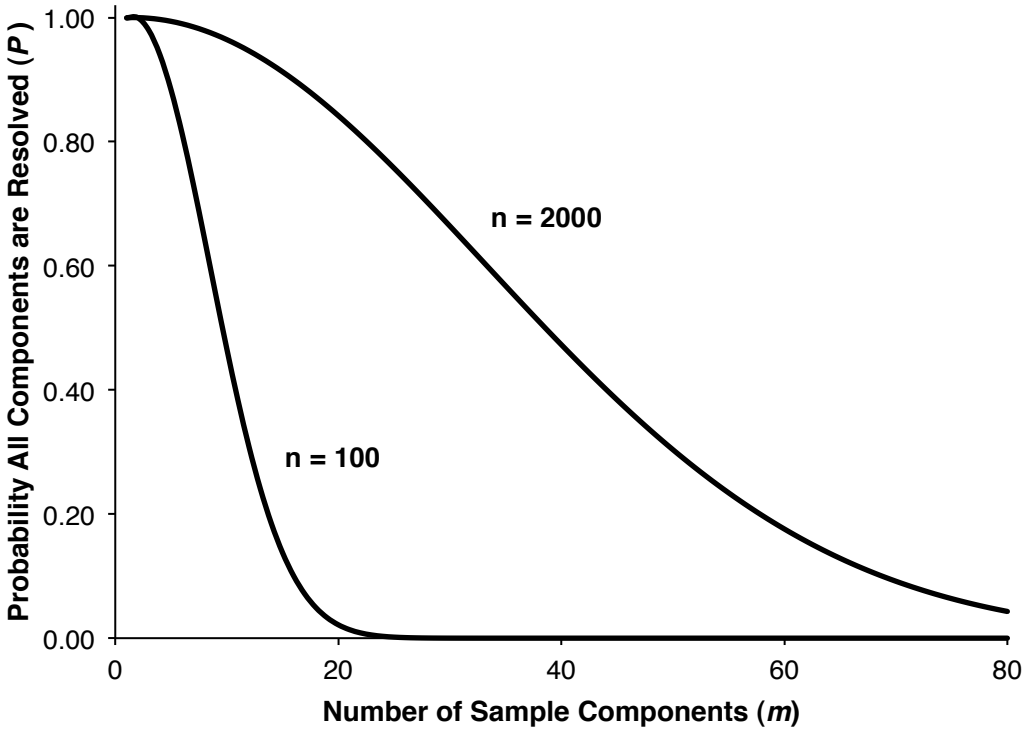

Figure 1.6. Equation 1.9 plotted as a function of number of sample components (m) at two given peak capacities (100 and 2,000). Equation 1.9 is adapted from ref. 97.

likely that the majority of sample components in a simple mixture will be resolved just by random chance with high peak capacity separation techniques, minimizing the time required for separation optimization. While some assumptions are made in this model that may not necessarily apply to real-life analyses, the idea remains the same. High peak capacity separations are advantageous in the analysis of simple mixtures, potentially drastically reducing the effort required for separation optimization.

Recent studies aimed at maximizing peak capacities in 1D gradient elution HPLC separations have reported values as high as ~500 in 2 hours, using a 60

cm long column with 5 μm pellicular particles at elevated temperatures,[98] and ~1500 in over 30 hours, using high pressure systems with 200 cm long columns packed with 3 μm porous particles,[99] for the analysis of complex peptide mixtures. It is clear that even specialized 1D HPLC systems cannot approach the large desired peak capacities within a reasonable analysis time (≤ 2 hours). Capillary zone electrophoresis (CZE) has become a popular separation technique for biomolecules in the past 20 years due to its high efficiency and decreased analysis times. Recently, a peak capacity of over 100 has been reported in just under 4.5 minutes for tryptic peptides using CZE.[100] However, 1D CZE separations still do not offer large enough peak capacities. The fact that conventional 1D separation techniques do not have peak capacities sufficient enough (> 1,500) within reasonable analysis times (≤ 2 hours) has forced researchers to develop other separation techniques capable of producing large peak capacities.

1.5.2 Two Dimensional (2D) Separation Theory

Several researchers have given insight into the potential for large peak capacities if two dimensional (2D) separations are considered.[101-103] As shown by Equation 1.10,

$$n_{c,2D} = n_{c,1} \times n_{c,2} \qquad (1.10)$$

the overall peak capacity of a two dimensional separation, $n_{c,2D}$, is equal to the product of the individual peak capacities of each dimension, $n_{c,1}$ and $n_{c,2}$. This is an absolute best-case scenario where the separation mechanisms are orthogonal, or in other words, the entire separation space is accessible to chromatographic peaks, and no sample resolution is lost upon transfer from the first dimension to the second. Actual peak capacities realized are lower than predicted by Equation 1.10 but its importance remains. Coupling separation techniques of moderate peak capacity (i.e.,100 and 20) has the potential to yield a large overall 2D peak capacity (2000).

In practical 2D work, the overall 2D peak capacity must be corrected for potential undersampling by the second dimension and the fractional coverage of the separation space, a function of orthogonality between the separation dimensions.

$$n'_{c,2D} = \frac{n_{c,1} \times n_{c,2} \times f}{\beta} \quad (1.11)$$

Equation 1.11[104] shows the dependence of the actual, or effective, 2D peak capacity, $n'_{c,2D}$, on the peak capacities of each dimension, $n_{c,1}$ and $n_{c,2}$, the fractional coverage of the separation space, f, and an undersampling correction factor, β.

To maximize the effective 2D peak capacity, the separation mechanisms chosen in each dimension of a two dimensional scheme must be orthogonal. In other words, the two separation mechanisms must be completely uncorrelated.[105]

The fractional coverage metric addresses the degree of orthogonality between dimensions by calculating the fraction of the separation space that is actually accessible to chromatographic peaks. Numerous methods for calculating fractional coverage have been evaluated.[104,106] A method borrowed from ecological home range studies has been applied to two dimensional separation spaces and has proven to be a good metric for determining fractional coverage.[104] The method involves calculating the smallest convex polygon that encompasses all peak positions in a two dimensional separation space (see Figure 1.7). The fraction of accessible separation space is found by simply dividing the area of the smallest convex polygon by the area of the separation space.

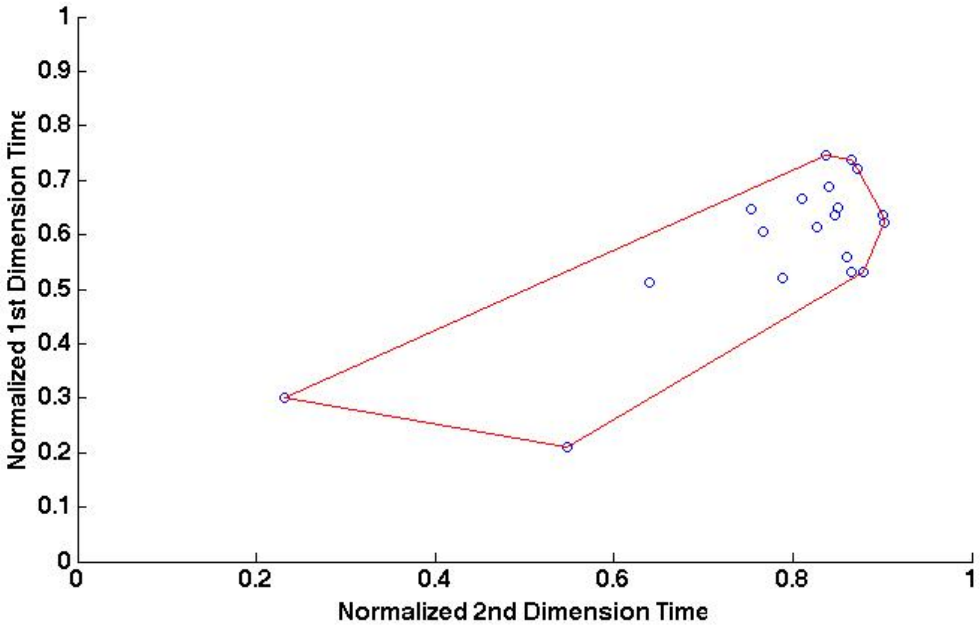

Figure 1.7. Minimum convex hull method applied to randomly placed chromatographic peaks in a normalized separation space. The fractional coverage was calculated to be ~14%. Chromatographic peaks only have access to ~14% of the total separation space.

The effect of undersampling on the effective two dimensional peak capacity is often overlooked in two dimensional work and can lead to severely inflated reported peak capacities. Murphy, Schure, and Foley reported the first major study quantifying the effect of undersampling.[107] The main finding states that peaks from the first dimension must be sampled at least 3-4 times by the second dimension over their 8σ base peak width to avoid a substantial loss in resolution of a pair of first dimension peaks. A more rigorous approach to determine the effect of undersampling in two dimensional work was taken by Davis, Stoll and Carr,[108] in which two dimensional separation spaces were simulated with samples of multiple components, random retention times, and random peak heights. The effect of undersampling on the number of observed peaks in the simulated separation spaces was the basis for Equation 1.12 given below.

$$\beta = \sqrt{1 + 3.35\left(\frac{t_s}{w_1}\right)^2} \qquad (1.12)$$

The undersampling correction factor, β, is a function of the 4σ width of a first dimension peak, w_1, and the second dimension sampling time, t_s. Further analysis of Equation 1.12 is discussed in Chapter 1, Section 5.4.

By calculating the fractional coverage and undersampling correction factor of a particular two dimensional separation scheme, the “product rule” shown in Equation 1.10 can be modified, as shown in Equation 1.11, to yield an effective, or actual, two dimensional peak capacity.

1.5.3 Peak Capacity Production Rates of Recent 2D Separation Schemes

Since the focus of some of this work is in maximizing effective 2D peak capacity in short analysis times, peak capacity production rate (peaks/min) will be used as the figure of merit when comparing separation schemes. The following section discusses some peak capacity production rates reported in two dimensional liquid chromatography, LC x LC, and in microfluidic based two dimensional separation schemes. It should be noted that these peak capacity production rates may not be, and likely are not, corrected for undersampling or fractional coverage. This implies that the reported peak capacity production rates are larger than truly achievable. Effort will be taken to make it clear how each peak capacity, and thus peak capacity production rate, was calculated.

Yates *et. al.*[109-113] have thoroughly described a technique known as multidimensional protein identification technology (MudPIT) in which a microcapillary column is packed with both strong cation exchange (SCX) material and reversed phase (RP) material. Samples are eluted through the first dimension SCX separation with a step-gradient of buffer with increasing ionic strength, and subsequently separated by RP with a linear gradient of acetonitrile. Peak capacity production rates of ~36 peaks/min have been reported during a 90 minute separation.[112] It should be noted, however, that the true value of this technique is its ability to be coupled to mass spectrometry (MS). Stoll and Carr[22] have described a fast, comprehensive 2D HPLC (LC x LC) separation of tryptic peptides from bovine serum albumin (BSA) in which a SCX column in the first

dimension is coupled to a RP column, thermostated at 100ºC, in the second dimension. Peak capacity production rates of ~67.5 peaks/min have been reported using this separation scheme. In both of these 2D HPLC reports, the peak capacities reported do not account for potential undersampling or fractional coverage of the two dimensional separation space. The effective peak capacity production rates are likely lower than reported.

Microfluidic based 2D separation schemes have become increasingly popular as the field of microfluidic based separations grows. Numerous reports of coupling electrophoretic techniques in two dimensional schemes on microfluidic devices have been reported. Ramsey *et. al.* have reported peak capacity production rates as high as ~280 peaks/min on a microfluidic device utilizing micellar electrokinetic chromatography (MEKC) followed by zone electrophoresis (ZE) for analysis of tryptic digests.[114,115] Other separation methods that have been described include capillary gel electrophoresis coupled with micellar electrokinetic chromatography (CGE-MEKC),[116,117] with peak capacity production rates of ~84 peaks/min, and isoelectric focusing coupled with zone electrophoresis (IEF-ZE),[118] with peak capacity production rates of ~25 peaks/min.

Microfluidic two dimensional schemes coupling liquid chromatography with electrophoresis have recently been reported as well. Chambers et. al. reported integration of reversed phase liquid chromatography and capillary zone electrophoresis on a microfluidic device capable of producing a peak capacity of

640 in 30 minutes, or a peak capacity production rate of ~21 peaks/min.[119] It should be noted that the focus of this work was not only the coupling of reversed phase liquid chromatography with capillary zone electrophoresis on a microfluidic device, but also the integration of electrospray ionization off the corner of the device for detection with mass spectrometry. More recently, capillary liquid chromatography has been interfaced with microfluidic capillary electrophoresis, again with electrospray ionization, for analysis of complex peptide mixtures.[120] Peak capacity production rates of ~28 peaks/min were reported. The peak capacity production rates reported for the microfluidic based two dimensional schemes were not corrected for undersampling or fractional coverage.

1.5.4 Advantages of μFFE as a Second Dimension Separation Technique

The effect of undersampling on the effective peak capacity of a 2D separation scheme can be drastic. Figure 1.8 shows the relationship between the fraction of first dimension peak capacity retained after sampling by the second dimension, $1/\beta$, and second dimension sampling time, t_s. The undersampling correction factor, β, is determined from Equation 1.12 as a function of second dimension sampling time, t_s.

If the goal is to maximize effective peak capacity in a short analysis time, it is clear the second dimension sampling time must be fast. For example, if the 10 minute first dimension separation is considered in Figure 1.8, a second dimension sampling time of ~10 seconds would decrease the peak capacity

achieved in the first dimension by ~70%. Discrete separation techniques (or separations in time) are not the ideal choice for second dimensions in a two dimensional separation scheme. If the second dimension separation time is to be sped up to decrease the second dimension sampling time, it is done so at the

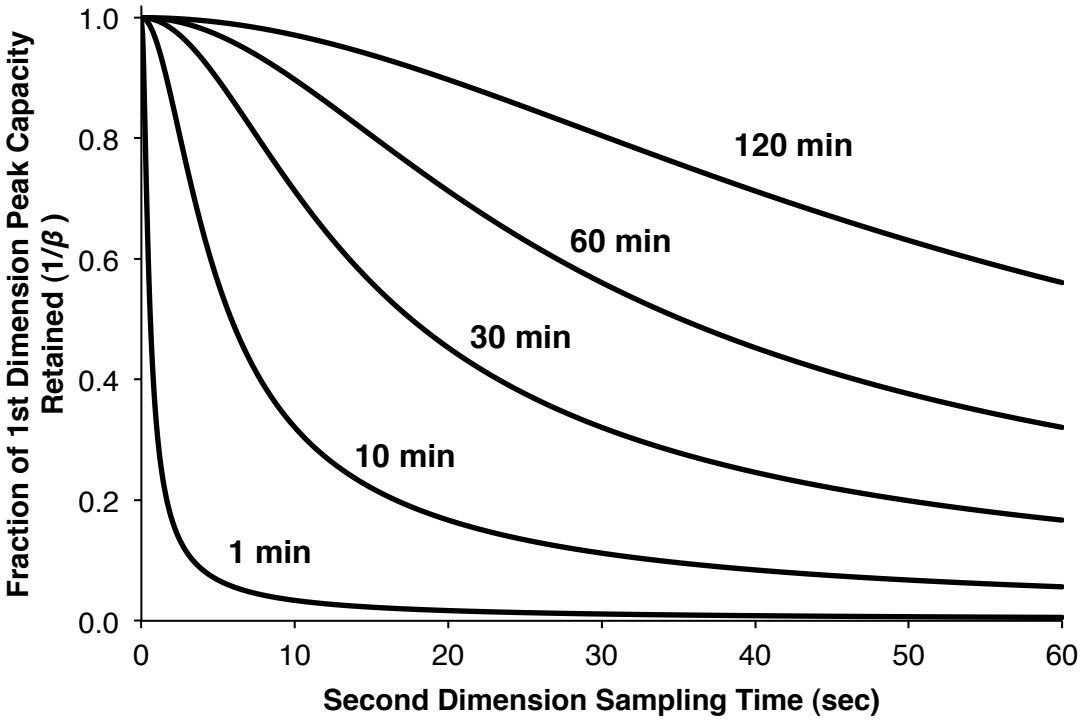

Figure 1.8. Plot of fraction of first dimension peak capacity retained after sampling by the second dimension ($1/\beta$) versus second dimension sampling time (t_s) for first dimension separation times of 1, 10, 30, 60, and 120 minutes assuming a first dimension efficiency of 150,000 theoretical plates.

expense of second dimension peak capacity. This leads to an optimum second dimension sampling time where the effective 2D peak capacity is maximized.[121]

Discrete separation techniques (or separations in time) will ultimately have some minimum time required for adequate separation to occur. The ideal second

dimension separation technique would be one in which the first dimension separation can be sampled very quickly and the peak capacity is not time-dependent. Micro free flow electrophoresis as a second dimension separation technique satisfies these criteria. Micro free flow electrophoresis is a separation in space, not time, so the peak capacity produced is not time dependent. Also, since the separation is continuous in nature, the second dimension sampling time is ultimately determined by time required for adequate sample detection (generally 100-500 milliseconds for our detection scheme). At second dimension sampling times of 100-500 milliseconds, the loss of peak capacity due to undersampling is essentially nonexistent. For example, if the 10 minute first dimension separation is again considered in Figure 1.8, a second dimension sampling time of 500 milliseconds would decrease the peak capacity achieved in the first dimension by only ~1%. It is clear that μFFE is an ideal choice for a second dimension separation in a two dimensional scheme, assuming orthogonal separation mechanisms are used.

Micro free flow electrophoresis is also a good choice for a second dimension separation in a two dimensional scheme because of the flexibility in electrophoretic separation modes that can be employed. In general, most electrophoretic modes that have been employed on capillary including zone electrophoresis (ZE), micellar electrokinetic chromatography (MEKC), and isoelectric focusing (IEF), can also be employed on a μFFE device. Numerous

reports of micro free flow zone electrophoresis (μFFZE) are detailed in the literature.[51,52,56-59,62,74,91,122,123]

Micellar electrokinetic chromatography (MEKC) is an electrophoretic separation mode that incorporates micelles in the electrolyte buffer that act as a pseudo-stationary phase and is often used to separate neutral species or species that may be difficult to separate by zone electrophoresis. Separation arises between neutral species due to differences in partitioning into and out of the micelles. Micro free flow micellar electrokinetic chromatography (μFFMEKC) has not been described in detail in the literature but is certainly an option for second dimension separations in a two dimensional scheme.

Isoelectric focusing (IEF) is an electrophoretic separation mode utilizing a pH gradient to separate analytes based on their isoelectric points (pI), or the pH at which they have zero net charge. Isoelectric focusing is fundamentally different than either zone electrophoresis or micellar electrokinetic chromatography in that it is a focusing technique. Separation performance is not hindered by traditional band broadening factors such as injection width and longitudinal diffusion. Instead, the ability to separate analytes is a function of the slope of the pH gradient and, of course, the applied electric field. Isoelectric focusing in capillary format is unique among electrophoretic separation modes because it is a separation in space, not time. It is not surprising then that isoelectric focusing has been one of the most popular separation modes in μFFE devices. Numerous reports of micro free flow isoelectric focusing (μFFIEF) for a

variety of analytes have been detailed in the literature, including separations of peptides,[124] proteins,[61] and subcellular organelles.[89]

It is clear that a number of separation modes are available when using μFFE devices as second dimension separation techniques in two dimensional schemes, ultimately improving the likelihood that orthogonal separation mechanisms can be used in each dimension.

1.6 Scope of Thesis

Micro free flow electrophoresis technology has progressed considerably in the past decade and use of the technique for analytically relevant applications has grown in recent years.[125,126] However, this introduction has pointed out that two key areas of improvement must be addressed for μFFE devices to reach their full potential in long term continuous monitoring and as a second dimension in a two dimensional separation scheme. Chapter 2 will detail a simple, yet effective, way for mitigating the effects of electrolysis bubbles on analyte stream stability in μFFE by addition of surfactant or organic modifier to the electrolyte carrier buffer. The longest stable μFFE separation performed on our devices is shown to support the effectiveness of this approach. Chapter 3 will detail an approach for making zero dead volume connections to μFFE devices. This chapter will culminate with the first two dimensional separation performed with μFFE as the second separation dimension. Chapter 4 will detail the fabrication

and operation of a monolithic microchip electrophoresis-micro free flow electrophoresis device for seamless integration of two separation dimensions. The first electrokinetically gated injection on an anodically bonded all glass device will be discussed. Chapter 5 will give a summary of the thesis and provide a future outlook for μFFE devices and separations.

Chapter 2

Using Buffer Additives to Improve Analyte Stream Stability in Micro-Free Flow Electrophoresis

"Frost, N. W. and Bowser, M. T. *Lab Chip* **2010,** *10* (10), 1231-1236."

2.1 Summary

Micro-free flow electrophoresis (μFFE) is a separation technique that continuously separates analyte streams as they travel through an electric field applied perpendicularly to the flow in a microdevice. Application of the technique has been limited by the generation of electrolysis bubbles at the electrodes, which results in unstable flow paths through the device. This work introduces the use of surfactants and nonaqueous solvents in the carrier buffer as a means of increasing stability of separated analyte streams. Adding surfactant or nonaqueous solvents lowers the surface tension of the carrier buffer, which we hypothesize promotes the formation of smaller electrolysis bubbles. A 6-fold improvement in the standard deviation of analyte stream position was observed upon addition of 10 mM SDS. Likewise, an approximately 12-fold improvement in stability was observed upon addition of 300 μM Triton X-100. Similar stability improvements were found in carrier buffers containing nonaqueous solvents. An 8-fold improvement in stability was found with a carrier buffer containing 50% methanol and a 6-fold improvement was found with a carrier buffer containing 37.5% acetonitrile. Long-term use was demonstrated with a carrier buffer containing 300 μM Triton X-100 in which separated analyte streams remained stable for nearly two hours.

2.2 Introduction

Free-flow electrophoresis (FFE) is an electrophoretic separation technique used to continuously separate a stream of charged analytes.[48] Briefly, a sample is continuously streamed into a planar flow channel. An electric field is applied perpendicularly to the pressure driven flow and analyte streams are deflected laterally according to their mobility. Since its inception over fifty years ago,[37,38] FFE has been used to separate a wide range of analytes including cell populations,[45,46,127] liposomes,[44,128] enzymes,[39,129] and proteins for proteomic applications.[130-133]

A drawback of conventional FFE is the significant Joule heating that results from the poor heat dissipation of the relatively large flow channel. This heating limits the potential that can be applied to 60-90 V/cm.[49], [50] Miniaturization of FFE onto microscale formats, which increases the surface-area-to-volume ratio of the separation chamber, has proven to allow better heat dissipation than preparative scale FFE devices. Raymond *et al.*[51] introduced the first μFFE device, fabricated in silicon, in 1994. This device demonstrated Joule heating improvements over preparative FFE devices, however the electrical breakdown voltage of this silicon device limited the potential that could be applied across the separation channel to 100 V. Since then, μFFE devices have been fabricated using substrates that accommodate higher field strengths including polydimethylsiloxane (PDMS),[62] and glass.[58,59] Electric fields as high as 589 V

cm^{-1} have been reported using an all glass device before significant Joule heating occurs.[57] Device performance is no longer limited by achievable electric field strengths, but rather by electrolysis bubbles formed during electrophoretic separation.

In order for μFFE devices to utilize their continuous nature in long term continuous monitoring applications or as a second dimension separation in a two dimensional separation scheme, new strategies to mitigate the effects of electrolysis bubbles on the stability of separated analyte streams must be explored. Decreasing the surface tension of aqueous buffers has been shown to have favorable effects on minimizing bubble size during electrolysis. For example, addition of surfactant to aqueous buffers has been shown to decrease the size of bubbles generated at electrode surfaces.[134] Addition of an organic solvent has produced similar results.[135,136] Likewise, addition of surfactant or organic solvent has been shown to stabilize bubbles and increase coalescence time,[137,138] effectively keeping smaller bubbles from combining into larger ones. In this work, we examine the effect of two surfactants (anionic sodium dodecyl sulfate and nonionic Triton X-100) and two organic solvents (methanol and acetonitrile) on the stability of separated analyte streams in a μFFE device.

2.3 Experimental

2.3.1 Chemicals and Reagents

Deionized water (18.3 MΩ, Barnstead, Dubuque, IA) was used for all buffer and sample preparations. HPLC-grade methanol (≥99.9%) was obtained from Sigma-Aldrich (St. Louis, MO). HPLC-grade acetonitrile (≥99.8%) was obtained from Mallinckrodt (Paris, KY). HEPES was obtained from Alfa Aesar (Heysham, Lancashire, UK) in 99% purity. Triton X-100 and sodium dodecyl sulfate (SDS, ~99%) were obtained from Sigma-Aldrich. Buffers were adjusted to appropriate pH by addition of 50% NaOH obtained from Sigma-Aldrich. Aqueous buffers were vacuum filtered through a 0.2 µm nitrocellulose membrane filter (Fisher Scientific, Fairlawn, NJ) before use. Disodium fluorescein (Acros Organics, NJ), rhodamine 123 chloride (Sigma-Aldrich), and rhodamine 110 (Sigma-Aldrich) were prepared in 190 proof ethanol (Fisher Scientific) and diluted in separation buffer. Piranha solutions (4:1 H_2SO_4/H_2O_2)(Ashland Chemical, Dublin, OH) were used to clean glass wafers and etch unwanted Ti. GE-6 (Acton Technologies, Inc., Pittston, PA) was used to etch unwanted Au. Concentrated HF (49%)(Ashland Chemical) was used to etch the glass wafers. Silver conductive epoxy (MG Chemicals, Surrey, BC, Canada) was used to make electrical connections to the µFFE device.

2.3.2 Device Fabrication

A multiple depth µFFE chip was fabricated as previously described.[59]

Briefly, 58 μm deep electrode channels were etched into a 1.1 mm borofloat wafer (Precision Glass & Optics, Santa Ana, CA) using standard photolithography techniques. A second photolithography procedure defined the remaining features, leaving a 20 μm deep × 1 cm wide × 2.5 cm long separation channel and 78 μm deep electrode channels. A 150 nm thick layer of Ti was deposited by a Temescal electron beam evaporator, followed by a 150 nm thick layer of Au. A final photolithography and etching procedure was used to remove the unwanted Ti and Au to define the electrodes. A second wafer with pre-drilled access holes and a ~90 nm thick layer of amorphous silicon (aSi) was aligned with the featured wafer and anodically bonded (900 V, 3 h, 450 ºC, 5 μFFE) using a Karl Suss SB-6 wafer bonder (Munich, Germany). Nanoports (IDEX, Oak Harbor, WA) were attached over access holes for fluidic connections. Silver conductive epoxy was used to attach lead wires to the electrodes. The chip was perfused with 1M NaOH to remove aSi from the channels.

2.3.3 Separation Conditions

Syringe pumps (Harvard Apparatus, Holliston, MA) were used to pump separation buffer through the chip at a flow rate of 0.4 mL/min (~0.13 cm/sec in the separation channel) and sample into the sample inlet at 50 nL/min (~0.12 cm/sec in the separation channel). SDS and Triton X-100 stability studies were performed with 150 V applied to the right electrode while the left electrode was held at ground. Long-term Triton X-100 studies were performed with an applied voltage of 40 V. Methanol and acetonitrile stability studies were performed with

an applied voltage of 75 V. 25 mM HEPES at pH 7.00 was used for SDS and Triton X-100 experiments. 10 mM HEPES at pH 7.50, 10 mM HEPES in methanol at pH* 7.50, and 10 mM HEPES in 75:25 acetonitrile/water at pH* 7.50 were used in the mixed solvent experiments. (Note: pH values listed for methanol and acetonitrile solutions are apparent values as measured by a pH meter and are only used to ensure reproducibility of the preparation) Aqueous and nonaqueous buffers were mixed to yield the following ratios: water/methanol (100/0, 85/15, 70/30, 50/50, 30/70, 15/85, 0/100) and water/acetonitrile (100/0, 88.75/11.25, 77.5/22.5, 62.5/37.5, 52.5/47.5, 25/75). Sample consisted of fluorescein (250 nM), rhodamine 123 (250 nM), and rhodamine 110 (125 nM) diluted in separation buffer. Rhodamine 123 was excluded from Triton X-100, methanol, and acetonitrile stability studies to simplify data analysis.

2.3.4 Instrumentation, Data Collection and Processing

The separation channel was imaged using a QuantEM:512SC CCD camera (Photometrics, Tucson, AZ) attached to a SMZ1500 stereomicroscope (Nikon Corp., Tokyo, Japan) with a 1.6x objective lens. The microscope was equipped with an Endow GFP bandpass emission filter cube (Nikon Corp.) containing two bandpass filters (450-490 and 500-550 nm) and a dichroic mirror with a 495 nm cutoff. The microscope was focused (0.75x zoom) on a region ~1.4 cm downstream from the sample inlet. Laser induced fluorescence (LIF) detection performed using a 150 mW, Argon-ion laser (Melles Griot, Carlsbad, CA) expanded into a ~2.5 cm x ~150 μm line across the separation channel. The

entire instrument setup was enclosed in black, rubberized fabric (Thorlabs, Newton, NJ). Micromanager software with Image J was used for imaging (camera gain 3, intensity 1000) and linescan acquisition. All linescans were one pixel in width. During SDS stability studies, images were recorded every 500 milliseconds for approximately 3.75 min. During long term Triton X-100 studies, images were acquired every 30 seconds for 2 hours. During Triton X-100, methanol, and acetonitrile stability studies, images were acquired every 250 milliseconds for approximately 3.75 minutes. The exposure time was varied to ensure a strong signal. Linescan data was processed using an in-house made LabView program. Individual linescans were analyzed using Cutter 7.0.[139]

2.4 Results and Discussion

2.4.1 Surfactants

Figure 2.1A is a 2D contour diagram that plots the linescans of multiple μFFE separations recorded over time. In this case, 800 linescans were recorded over a period of approximately 4 minutes. This format is useful for tracking variations in μFFE stream position over time. The erratic behavior of the stream positions shown in Figure 2.1A is typical of those observed under conditions where electrolysis bubbles are forming at the electrodes. Formation of a bubble restricts flow on one side of the device shifting the analyte streams in the opposite direction. Clearance of the bubble removes the restriction causing a sudden shift of the streams back to their original position. Once bubbles start to

form in the system this behavior is random making prediction of stream position extremely difficult.

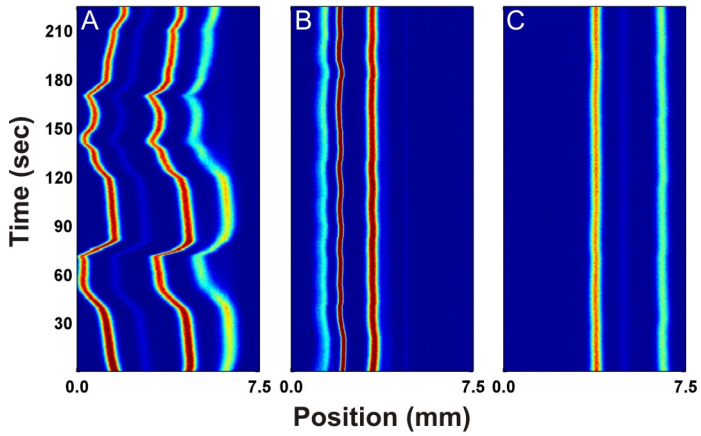

Figure 2.1. Contour plots illustrating analyte peak position over 4 minutes (i.e. 800 consecutive linescans) in the separation chamber of the µFFE device with a carrier buffer containing 25 mM HEPES at pH 7.00 with no surfactant (A), 10 mM SDS (B), and 300 µM Triton X-100 (C). The anode is on the left side of the images. The identities of the analyte bands from left to right are: fluorescein, rhodamine 110 impurity, rhodamine 110, and rhodamine 123. Note that rhodamine 123 was removed from the separation mixture in (C) for clarity.

Figure 2.1B shows the same µFFE separation with the addition of 10 mM SDS to the carrier buffer. Note that the addition of SDS increased the ionic strength of the buffer, increasing current in the device from 0.35 mA without SDS to 0.74 mA with 10 mM SDS. This increase in current means electrolysis increased two-fold with the addition of SDS, yet the stream positions remained stable. Figure 2.1C shows the same separation conditions where SDS is replaced with 300 µM Triton X-100, a nonionic surfactant. Again, the positions of

the analyte streams remain constant throughout the course of the analysis. The addition of a nonionic surfactant like Triton X-100 does not change the conductivity of the carrier buffer, but does act to lower the surface tension. Intuitively, nonionic surfactants seem to be the best option for improving the stability of analyte streams because they lower the surface tension of the carrier buffer without increasing the overall conductivity.

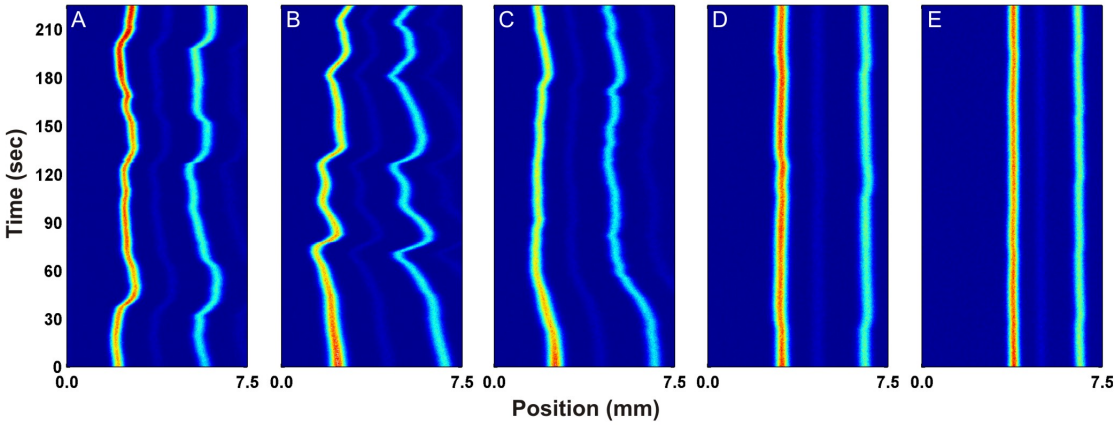

Figure 2.2. Contour plots illustrating analyte peak position over 4 minutes (800 consecutive linescans) in the separation chamber of the μFFE device with a carrier buffer of 25 mM HEPES at pH 7.00 containing 0 μM (A), 5 μM (B), 30 μM (C), 100 μM (D), and 300 μM (E) Triton X-100. The anode is on the left side of the images. The identities of the analyte bands from left to right are: fluorescein, rhodamine 110 impurity, rhodamine 110, and traces of rhodamine 123.

Figure 2.2 shows the effect of increasing Triton X-100 concentration on the separation of two fluorescent dyes (rhodamine 110 and fluorescein). Figure 2.2A shows the separation without Triton X-100 in the carrier buffer. The positions of the analyte streams shift erratically throughout the course of the

analysis. The addition of 5 μM Triton X-100 to the carrier buffer (Figure 2.2B) does not have a significant effect on analyte stream stability. Figure 2.2C shows the separation with the addition of 30 μM Triton X-100 to the carrier buffer. There is a noticeable improvement in stream stability as compared to Figures 2.2A and 2.2B. After an initial shift in position over the first minute of separation time, the analyte streams show only minor fluctuations in position over the remaining three minutes. Figure 2.2D shows the separation with the addition of 100 μM Triton X-100 to the carrier buffer. Clearly, the addition of 100 μM Triton X-100 improves the stability of the analyte streams significantly compared to separation conditions with no added surfactant. Figure 2.2E shows the separation upon the addition of 300 μM Triton X-100 to the carrier buffer. The stability of the analyte streams improves even further with almost no fluctuations in position over the course of the analysis. An addition of 1500 μM Triton X-100 to the carrier buffer was also tested (data not shown) and yielded a similar result to that as shown in Figure 2.2E.

The standard deviation of the position of the fluorescein stream over a period of 4 minutes (800 consecutive linescans) was plotted versus Triton X-100 concentration in Figure 2.3A. Clearly, stream position stabilizes with increasing Triton X-100 concentrations up to approximately 100-300 mM. This corresponds well with the reported critical micelle concentration (CMC) of 240 μM for Triton X-100.[140,141] It is well known that addition of surfactant to aqueous solutions decreases surface tension as the concentration approaches the CMC.[142]

Jańczuk *et al*. have measured the relationship between Triton X-100 concentration and surface tension in aqueous solutions.[143] They demonstrated a dramatic reduction in surface tension at Triton X-100 concentrations near the CMC (10-1000 mM). This is in excellent agreement with the range of Triton X-100 concentrations that yielded the most improvement in analyte stream stability.

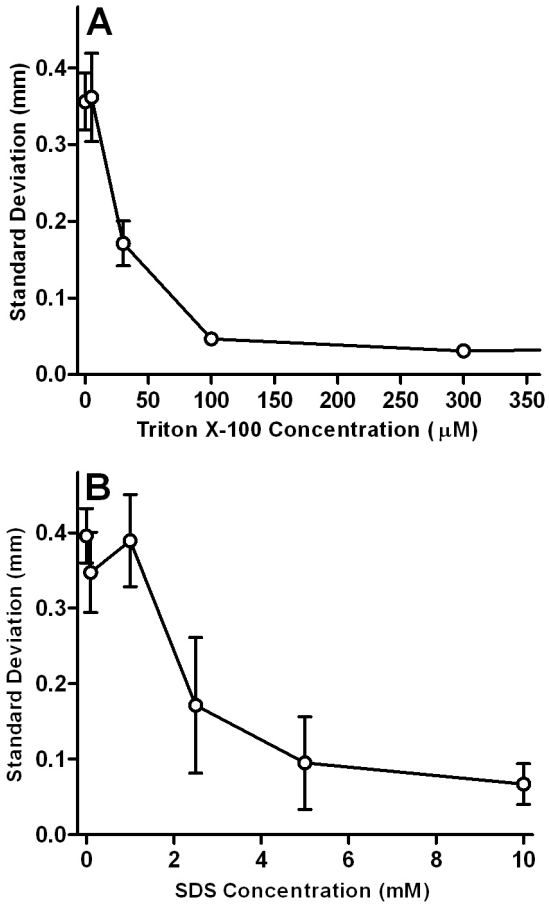

Figure 2.3. Plots of the standard deviation of fluorescein peak position recorded over 4 minutes versus surfactant concentration for Triton X-100 (A) and SDS (B). Error bars are the standard error of the mean, n = 3.

We hypothesize that this reduction of surface tension promotes formation of smaller bubbles, which have less effect on the stability of the analyte streams. At concentrations above the critical micelle concentration (CMC), the surface tension of the carrier buffer no longer decreases and stability doesn't show further improvement. It should be noted that the standard deviation recorded at 1500 μM Triton X-100 (not shown) is not statistically different from the data point at 300 μM at a 95% confidence level, indicating that the stability of the analyte streams is independent of surfactant concentration above the CMC.

A similar plot of standard deviation versus concentration of SDS is shown in Figure 2.3B. The reported CMC of SDS in pure water is 8 mM.[144,145] Lunkenheimer *et al*. have demonstrated that surface tension of aqueous solutions decreases as SDS concentration increases from 1 to 10 mM.[146] Again, this is in excellent agreement with the range of SDS concentrations where improvement in stream stability was observed. At concentrations above their respective CMCs, the standard deviation of the fluorescein stream in a carrier buffer containing Triton X-100 is approximately 50% lower than that of fluorescein in a carrier buffer containing SDS. The data clearly suggests that Triton X-100 is a better option for increasing the stability of separated analyte streams when compared to SDS due to the lower current generated and the lower amount of additive required to achieve stable flow streams.

2.4.2 Mixed Solvents

It appears that a reduction in surface tension is the key parameter in minimizing the effect of electrolysis bubbles on analyte stream stability. Changing the buffer solvent, as means of decreasing surface tension, should show a similar effect. Increasing the nonaqueous fraction in a mixed aqueous/nonaqueous carrier buffer decreases the surface tension of the buffer, similar to adding a surfactant.[147] Figure 2.4A shows the separation of two fluorescent dyes, rhodamine 110 and fluorescein, in 10 mM HEPES at pH 7.50 in water. The position of the analyte streams slowly drifts towards the cathode throughout the separation. Figure 2.4B is recorded using the same separation conditions as in Figure 2.4A but with 10 mM HEPES in 50:50 water/methanol at an apparent pH of 7.50. The stability of the analyte streams improves greatly

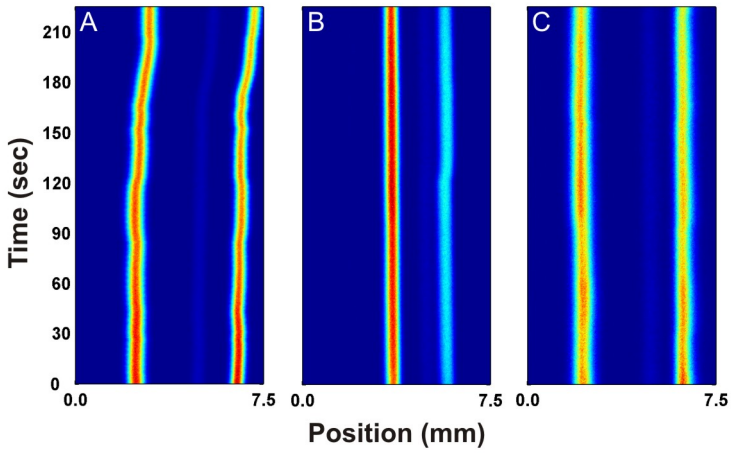

Figure 2.4. Contour plots of 800 consecutive linescans across the separation chamber of the µFFE device with a carrier buffer of 10 mM HEPES at pH 7.50 (A), 10 mM HEPES in 50:50 Water/Methanol at pH* 7.50 (B), and 10 mM HEPES in 62.5:37.5 Water/Acetonitrile at pH* 7.50 (C).

compared to the aqueous carrier buffer, showing only minor fluctuations in position over the course of the 4-minute analysis. It is clear that the addition of methanol to the carrier buffer has a significant effect on improving the stability of the analyte streams. Similar experiments were performed with acetonitrile as the nonaqueous component. Figure 2.4C shows the same separation conditions as in Figure 2.4A but with 10 mM HEPES in 62.5/37.5 water/acetonitrile at an apparent pH of 7.50 as the carrier buffer. Again, the positions of the analyte streams become more stable than in pure aqueous carrier buffer.

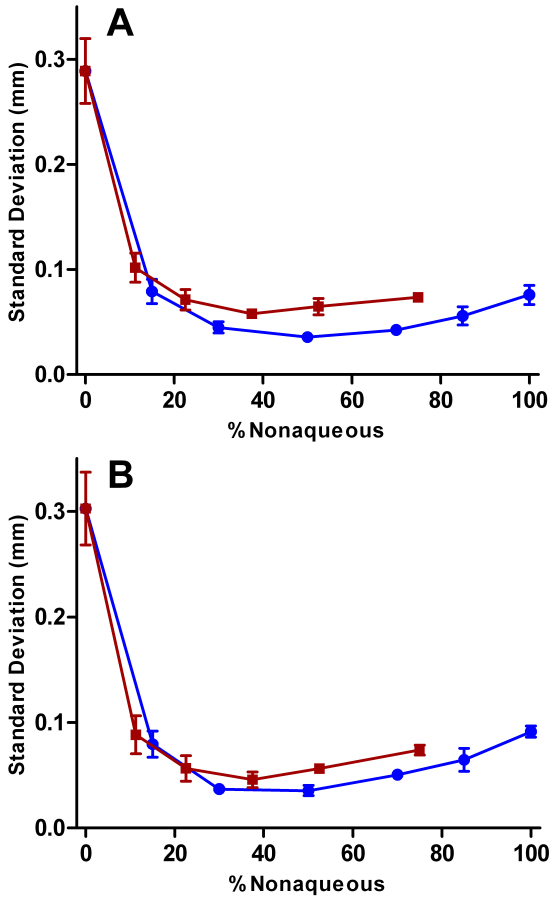

Figure 2.5. Plots of standard deviation of peak maxima versus nonaqueous percentage in carrier buffer for methanol (blue circles) and acetonitrile (red squares). Error bars are the standard error of the mean, n = 3.

Figure 2.5 shows plots of standard deviation of peak position versus percentage of nonaqueous component in the carrier buffer for rhodamine 110 (A) and fluorescein (B). Increasing the methanol fraction (blue trace) in the carrier buffer improves the stability of the analyte streams until a 50:50 water/methanol mixture has ben reached. The stability of the analyte streams worsens slightly as the methanol fraction is increased further, up to 100% methanol. The reason for this may be that methanol has a lower electrolysis potential than water, assuming the current density remains constant.[148] Even though the surface tension of the carrier buffer continues to decrease, the lower electrolysis potential of methanol makes it easier for electrolysis bubbles to form, decreasing analyte stream stability.

A similar trend is observed with increasing percentage of acetonitrile in the carrier buffer (red traces in Figure 2.5). After an initial improvement in stability with the addition of 11.25% acetonitrile to the carrier buffer, the data remained fairly constant up to 75% acetonitrile. Data was not collected above 75% due to the limited solubility of HEPES in acetonitrile. The data suggests that addition of even relatively small fractions of nonaqueous solvent to the carrier buffer (~12-15%) achieves significant improvements in stream stability. Only minimal gains are observed as the nonaqueous fraction is increased further.

2.4.3 Long Term Stability

In order for μFFE to reach its full potential as a continuous monitoring device, micropreparative platform, or as a second dimension in 2D separation schemes, it is essential that long-term separation stability be achieved. To date, stable μFFE separations have been demonstrated over periods of minutes but longer separations have proven problematic.[74] Figure 2.6 shows the separation of three fluorescent dyes (rhodamine 123, rhodamine 110, fluorescein) recorded over the course of approximately 2 hours in 25 mM HEPES at pH 7.00 with 300 μM Triton X-100 included in the carrier buffer. The analyte streams remain

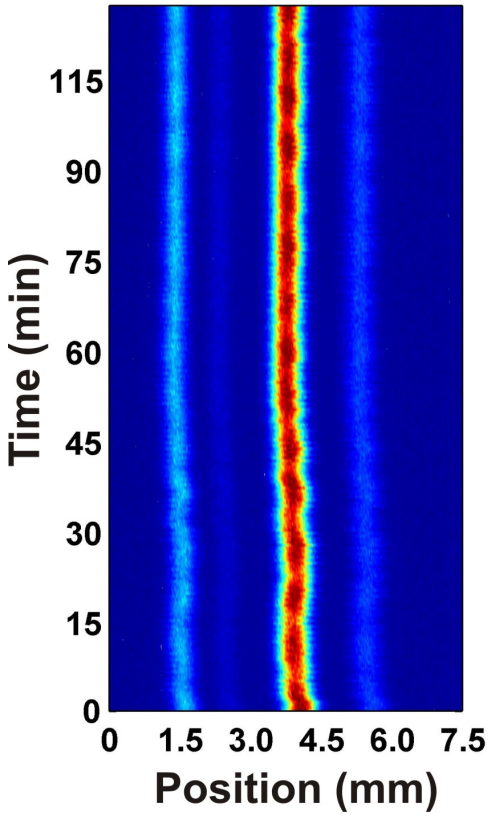

Figure 2.6. Contour plot of 235 consecutive linescans across the separation chamber over approx. 2 hours. From left to right: fluorescein, rhodamine 110 impurity, rhodamine 110, and rhodamine 123.

stable throughout the separation, with no major fluctuations in position. The ability to keep analyte streams in a constant position for prolonged periods of time opens up many possible uses for this device. Experiments requiring long-term monitoring are now possible with the addition of Triton X-100 to aqueous carrier buffers. Also, the ability to keep separated analyte streams stable lends itself to micropreparative separations. Macroscale FFE is used primarily for fractionation of complex samples and it now seems reasonable that μFFE could offer similar preparative options on a much smaller scale.

2.5 Conclusions

Lowering the surface tension of the carrier buffer dramatically improves the stability of analyte streams in μFFE. Addition of surfactants such as SDS or Triton X-100 to the aqueous carrier buffer improved the stability of the separated analyte streams. The nonionic surfactant Triton X-100 proved to stabilize the analyte streams more effectively than SDS, most likely due to the lower surface tension of aqueous Triton X-100 solutions and its nonionic nature, which doesn't increase the conductivity of the carrier buffer. The addition of methanol or acetonitrile to the carrier buffer had similar stabilizing effects. Addition of fractions of nonaqueous solvent above approximately 12% has been shown to improve the stability of analyte streams when compared to pure aqueous carrier buffers.

Chapter 3

Zero Dead Volume Capillary Connections to Micro Free Flow Electrophoresis Devices

3.1 Summary

In this work, an interface between capillaries and glass μFFE devices was developed that minimizes dead volume and allows for efficient transfer of sample bands across the interface. This interface utilizes an etched capillary insertion channel, which places the outlet of the capillary in the separation chamber of the μFFE device. The effectiveness of this interface was assessed by comparing peak widths upon transfer across the interface. No observable peak broadening was evident due to the interface. This interface was then used in a two dimensional separation scheme employing a homebuilt capillary electrophoresis first dimension separation and a μFFE second dimension separation. This scheme produced an unadjusted peak capacity of 900 in less than 4 minutes and all 16 components of the sample mixture were resolved without previous optimization of the separation conditions. The adjusted peak capacity of 30 indicates that other separation modes should be explored to maximize the fractional coverage of the two dimensional space.

3.2 Introduction

The ability to make fluidic connections to microfluidic devices with zero dead volume is often essential to maximizing device performance when the device is to be connected to the "outside world". In other words, in instances where sampling is performed off-device, or when coupling separation dimensions (as in this work), the performance of the device suffers when sample is allowed to remix at interfaces where substantial dead volume exists. The two applications discussed previously, long term continuous monitoring and two dimensional separations with a μFFE device as the second dimension, require that there is minimal remixing of sample at the device interface. In long term continuous monitoring, the goal is to continuously monitor concentration dynamics over time from an incoming sample stream. If the interface has substantial dead volume, mixing of the stream can occur and concentration dynamics can be severely blurred. In two dimensional separations, if the sample stream from the first dimension encounters a region of substantial dead volume during the transfer to the second dimension, remixing of the sample stream can occur causing a loss in sample resolution gained in the first dimension.

The most common method for making these types of connections to traditional microfluidic devices was introduced by Bings *et al.*[93] The method utilizes small diameter diamond tip drill bits to fabricate a capillary insertion channel into the side of the device, which has been aligned with an etched

channel (see Figure 1.5). A variation of this method was employed in this work where a capillary insertion channel was etched during device fabrication. This insertion channel was aligned with a narrower electrophoresis channel to recreate what was shown in Bings *et al.* This method produced poor results and alternate schemes were explored.

The goal of this work was to develop a strategy for making zero dead volume connections to μFFE devices. The effectiveness of the developed strategy was judged by evaluating the extent of peak broadening upon transfer across the interface. This zero dead volume connection was then used to perform a two dimensional separation of an amino acid mixture.

3.3 Experimental

3.3.1 Chemicals and Reagents

Deionized water (18.3 MΩ, Millipore, Billerica, MA) was used for all buffer and sample preparations. CAPS was obtained from Alfa Aesar (Heysham, Lancashire, UK) in 99% purity. Triton X-100 was obtained from Sigma-Aldrich. Buffers were adjusted to appropriate pH by addition of 50% NaOH obtained from Sigma-Aldrich. Aqueous buffers were vacuum filtered through a 0.22 μm nitrocellulose membrane filter (Fisher Scientific, Fairlawn, NJ) before use. The μFFE separation buffer consisted of either 20 mM CAPS adjusted to pH 10.00 with 50% NaOH with 300 μM Triton X-100 (Sigma-Aldrich) or 20 mM Gly-Gly

adjusted to pH 3.18 with 10 mM SDS. Disodium fluorescein (Acros Organics, NJ), Rhodamine 123 (Sigma-Aldrich), and Rhodamine 110 (Sigma-Aldrich) were prepared in 190 proof ethanol (Fisher Scientific) and diluted in separation buffer. AlexaFluor488 labeling of amino acids was performed following manufacturer's instructions (Invitrogen). Piranha solutions (4:1 H_2SO_4/H_2O_2)(Ashland Chemical, Dublin, OH) were used to clean glass wafers and etch unwanted Ti. GE-6 (Acton Technologies, Inc., Pittston, PA) was used to etch unwanted Au. Concentrated HF (49%)(Ashland Chemical) was used to etch the glass wafers. Silver conductive epoxy (MG Chemicals, Surrey, BC, Canada) was used to make electrical connections to the μFFE device.

3.3.2 Device Fabrication

Numerous multiple depth μFFE devices, of different designs, were fabricated similar to previously described devices.[59] However, significant changes to the device design were made and will be discussed in Section 3.4.2. As a general overview of the fabrication process, electrode channels were etched into a 1.1 mm borofloat wafer (Precision Glass & Optics, Santa Ana, CA) using standard photolithography techniques. A second photolithography procedure defined the remaining features, leaving a 1 cm wide × 2.5 cm long separation channel and deep electrode channels. Some devices required an initial photolithography step to define and etch a capillary insertion channel. A 150 nm thick layer of Ti was deposited by a Temescal electron beam evaporator,

followed by a 150 nm thick layer of Au. A final photolithography and etching procedure was used to remove the unwanted Ti and Au to define the electrodes. A second wafer with pre-drilled access holes and a ~90 nm thick layer of amorphous silicon (aSi) was aligned with the featured wafer and anodically bonded (900 V, 3 h, 450ºC, 5 mbar) using a Karl Suss SB-6 wafer bonder (Munich, Germany). Nanoports (IDEX, Oak Harbor, WA) were attached over access holes for fluidic connections. Silver conductive epoxy was used to attach lead wires to the electrodes. The chip was perfused with 1M NaOH to remove aSi from the channels. Capillaries were fixed in capillary insertion channels using Crystalbond 509 (SPI Supplies, West Chester, PA) by applying a vacuum at an outlet Nanoport while the device and Crystalbond 509 were on a 140ºC hotplate.

3.3.3 Device Operation

A plexiglass sample carousel was constructed by the University of Minnesota physics machine shop for holding buffer and sample vials during capillary electrophoresis separations (see Figure 3.1). A Spellman CZE1000R power supply was used to apply potentials to buffer and sample vials. The power supply and injection sequence were controlled using a BNC 2110 DAQ board (National Instruments, Austin, TX) and PCIe-6321 DAQ card (National Instruments, Austin, TX). All control operations can be performed from a single LabVIEW interface including manipulating the power supplies, performing sample injections, and triggering image acquisition.

3.3.4 Data Collection and Processing

The capillary and μFFE separation channel and were imaged using a QuantEM:512SC CCD camera (Photometrics, Tucson, AZ) attached to a SMZ1500 stereomicroscope (Nikon Corp., Tokyo, Japan) with a 1.6x objective lens. The microscope was equipped with an Endow GFP bandpass emission filter cube (Nikon Corp.) containing two bandpass filters (450-490 and 500-550 nm) and a dichroic mirror with a 495 nm cutoff. Laser induced fluorescence (LIF) detection was performed using a 150 mW, Argon-ion laser (Melles Griot, Carlsbad, CA) expanded into a ~2.5 cm x ~150 μm line across the separation channel or the capillary. The entire instrument setup was enclosed in black, rubberized fabric (Thorlabs, Newton, NJ) to minimize stray light. MetaVue software was used for imaging. The exposure time was varied to ensure a strong signal. Images were processed using an in-house MATLAB routine.

3.4 Results and Discussion

3.4.1 Homebuilt Capillary Electrophoresis

Figure 3.1 shows the homebuilt capillary electrophoresis instrument including the plexiglass sample and buffer carousel, capillary, high voltage cable, and μFFE device and optical detection scheme. To test the separation performance of the homebuilt capillary electrophoresis instrument, a sample consisting of AlexaFluor488 labeled glycine, γ-aminobutyric acid (GABA), and

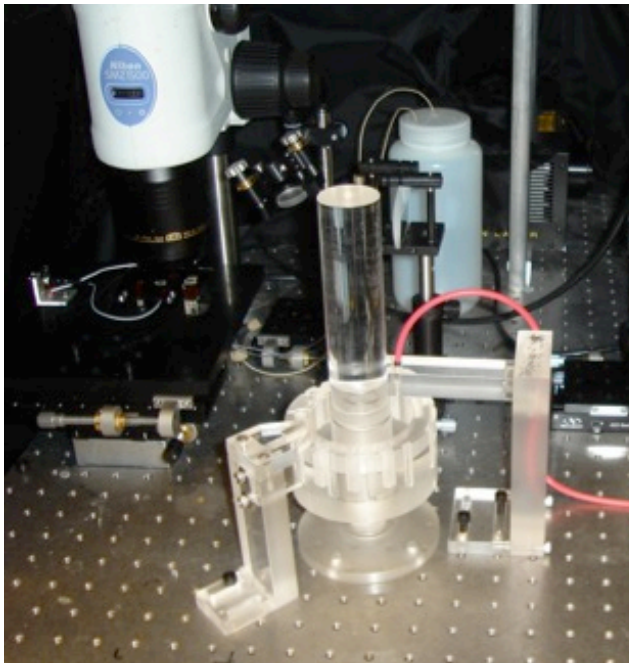

Figure 3.1. Homebuilt Capillary Electrophoresis Instrument. Components include a plexiglass sample vial carousel, high voltage cable and electrode, capillary connected to µFFE device, and laser induced fluorescence detection performed either on capillary or on device.

unreacted AlexaFluor488 dye was separated with on capillary detection prior to entering the µFFE device (an example of which is shown in Fig 3.2). The homebuilt capillary electrophoresis instrument routinely produced average theoretical plate numbers of 147,500 (n = 20, multiple days, by half-width). The instrument performance was satisfactory allowing the focus to turn to the interface between capillary and the µFFE device. The first dimension separation was monitored everyday on capillary prior to assessing the interface to ensure the separation was as expected.

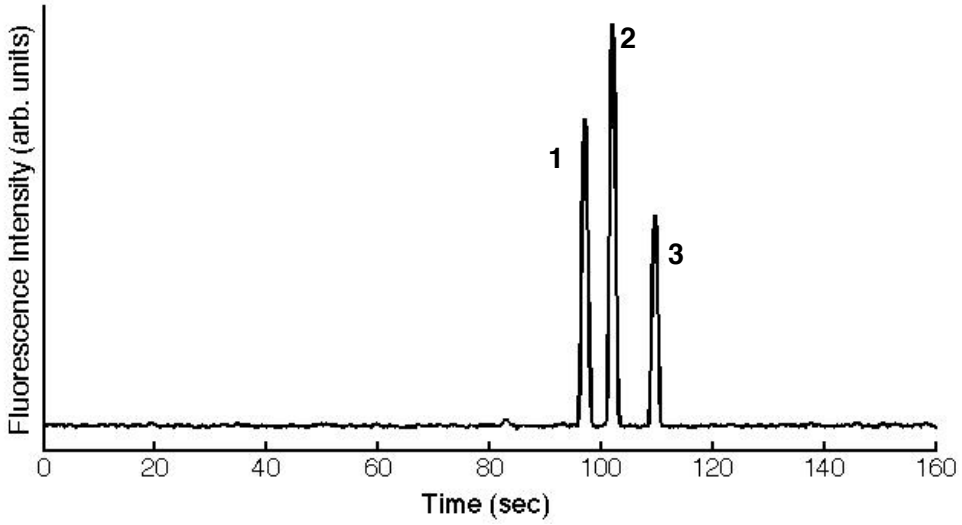

Figure 3.2. Homebuilt capillary electrophoresis separation of AlexaFluor488 labeled glycine, GABA, and unreacted dye on a 40 cm, 150 µm OD, 20 µm ID capillary at 25 kV with laser induced fluorescence detection on capillary immediately before entering µFFE device. Peak identification was not performed and peaks will be referred to as 1, 2, and 3 in order of migration.

3.4.2 Capillary - µFFE Coupling by Etched Capillary Insertion Channel

It should be noted that a number of interfaces and device designs were explored including using Nanoports™, aligning an access hole over an etched channel, and aligning a capillary with an etched channel, but all provided inadequate coupling between a capillary and µFFE devices. Results ranged from no observable flow (indicating that proper alignment was not achieved) to severely broadened peaks (indicating significant dead volume and sample remixing). These interfaces will not be discussed further.

Figure 3.3A is an image of the CAD file used to create the mask necessary to define the capillary insertion channel and the electrode channels

during photolithography. This is the first device design that allows for two µFFE buffer inlets (as opposed to a single µFFE buffer inlet as used in Chapter 2). The split µFFE buffer inlets allow the etching of a capillary insertion channel into the separation chamber of the device. The mask was used twice to separately define the capillary insertion channel and the electrode channels to achieve different etch depths (85 µm for the capillary insertion channel, 50 µm for the electrode channels). This was done by covering the unwanted mask features with electrical tape prior to photolithography. Figure 3.3B shows a completed device with a capillary inserted into the etched insertion channel and fixed with Crystalbond adhesive. The idea is that pressure driven flow in the µFFE device will flow around the inserted capillary to facilitate the transfer of fluid from the end of the capillary into the device.

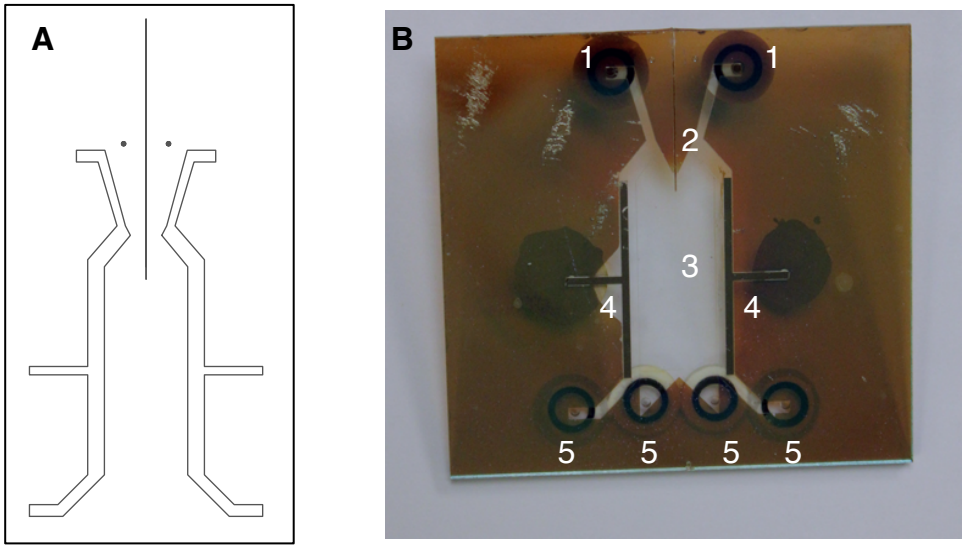

Figure 3.3. (A) New mask design to create a capillary insertion channel for a zero dead volume coupling to a µFFE device. (B) A completed µFFE device with (1) buffer inlets, (2) capillary insertion channel with capillary fixed inside, (3) µFFE separation chamber, (4) electrodes, (5) buffer outlets.

To test the quality of the fabricated interface, the 4σ peak widths of AlexaFluor488 labeled glycine, γ-aminobutyric acid (GABA), and unreacted AlexaFluor488 dye immediately before entering the μFFE separation space (detection on capillary) were compared to their 4σ peak widths immediately after entering the μFFE separation space (separation performed identical to Figure 3.2). It should be noted that peak identification was not performed so the peaks will be referred to as 1, 2, or 3 in order of migration time. From Figure 3.4, it is clear that this fabricated interface causes essentially no peak broadening upon transfer from capillary to μFFE device indicating minimal dead volume and remixing of the first dimension effluent. The 4σ peak widths of peaks 1, 2, and 3 immediately before entering the μFFE separation space, averaged from 4 replicate injections, were 1.95 seconds (5.1% RSD), were 2.05 seconds (4.9% RSD), and 2.10 seconds (5.5% RSD), respectively. The average 4σ peak widths (n = 6) of peaks 1, 2, and 3 immediately after entering the μFFE separation space were 1.95 seconds (5.1% RSD), 2.10 seconds (5.5% RSD), and 2.15 seconds (4.7% RSD), respectively. Statistically speaking, there is no observable broadening of the peaks upon transfer from capillary to the μFFE separation space. The successful zero dead volume coupling of μFFE devices to a capillary shown in this work will now allow these devices to be used for arguably their two most powerful applications, long term continuous monitoring and as a second dimension separation in a two dimensional separation scheme.

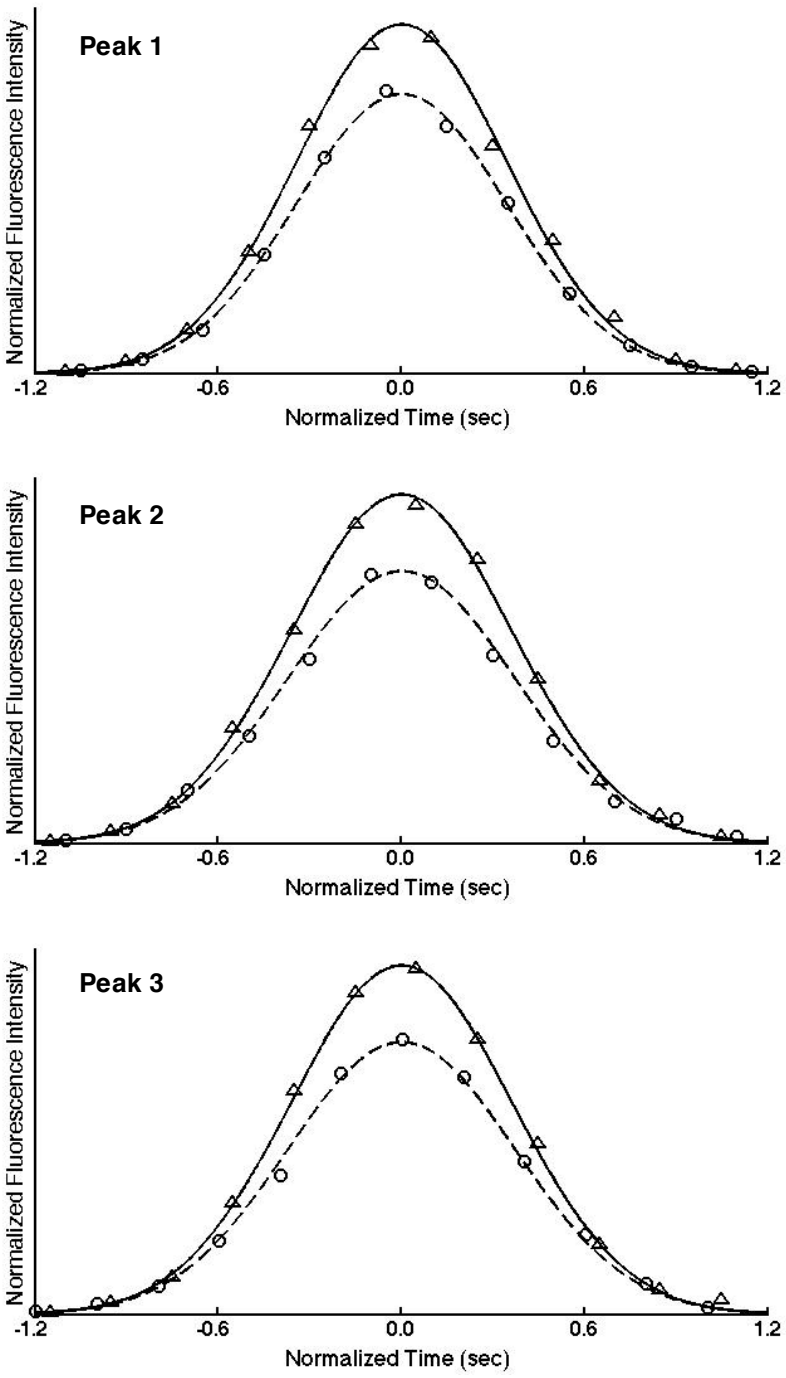

Figure 3.4. Comparison of Peaks 1, 2, and 3 (from Figure 3.2) immediately before entering the μFFE separation space (detection on capillary, triangles with solid line), and immediately after entering the μFFE separation space (detection on μFFE device, circles with dashed line). Curves are Gaussian fits to the experimental data shown. Time and fluorescence intensity have been normalized for ease of comparison.

3.4.3 Two Dimensional Separation of Amino Acids

To put this interface to the test, a two dimensional separation was performed. Figure 3.5 shows this first two dimensional separation utilizing μFFE as the second dimension separation technique. A first dimension capillary electrophoresis separation was coupled to a second dimension μFFE separation using the interface outlined in Section 3.4.2. The separation conditions are given in the caption. The sample consisted of 13 amino acids fluorescently labeled with

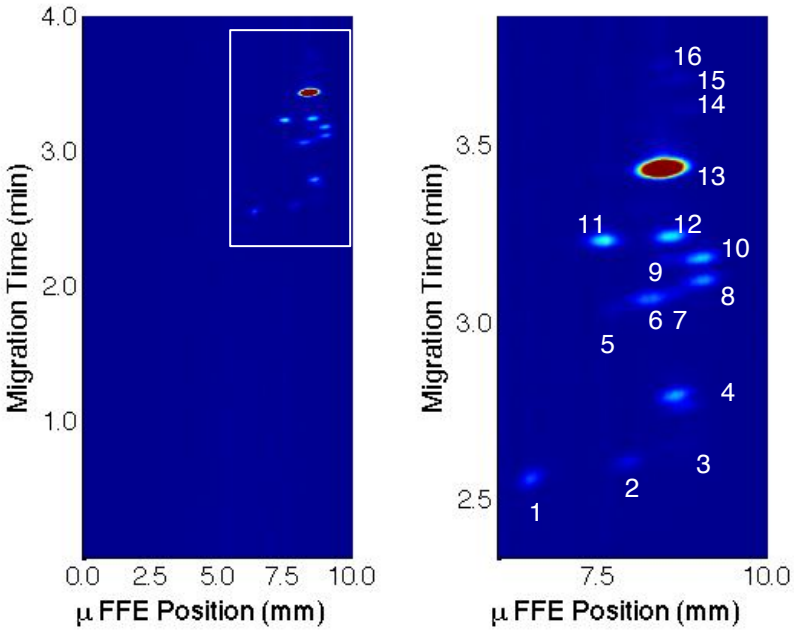

Figure 3.5. Contour plot of a two dimensional capillary electrophoresis – μFFE separation of 13 amino acids labeled with AlexaFluor 488 (16 components). CE separations were performed at an applied potential of 25 kV in a 40 cm long, 20 μm ID fused silica capillary with 20 mM CAPS pH 10.49 as the electrolyte buffer. Electrokinetic injections were performed at 5 kV for 5 seconds. The μFFE buffer consisted of 20 mM Gly-Gly pH 3.18 with 10 mM SDS pumped at a flow rate of 0.4 mL/min, with an applied voltage of 100 V. Images of the separation chamber 1.5 cm downstream from capillary outlet were collected at 5 Hz. The contour plot was created from 1,200 consecutive linescans. The image to the right is an expanded view of the area inside the white outline.

AlexaFluor488™ (ultimately yielding 16 components including unreacted dye and doubly labeled lysine-containing amino acids). The results of this two dimensional separation are quite promising considering that all 16 components of the mixture were resolved within 4 minutes with no optimization of the separation conditions. The power of high peak capacity separation techniques on the separation of relatively simple mixtures is quite apparent (as highlighted in Chapter 1, Section 1.5.1).

The unadjusted peak capacity of the two dimensional separation shown in Figure 3.5 was calculated to be 900 (60 in the first dimension, 15 in the second dimension) for an unadjusted peak capacity production rate of 3.9 peaks/sec (using the migration time of the last component). This peak capacity and peak capacity production rate are clearly inflated since very little of the separation space is actually available to component peaks (low fractional coverage). The adjusted peak capacity (using Equation 1.11, with $\beta = 0.98$ and $f = 3.34\%$, as calculated using the convex hull method) was 30 for an adjusted peak capacity production rate of 0.13 peaks/sec. It is clear that other combinations of separation modes should be explored to maximize the fractional coverage of the two dimensional space. This work shows that high peak capacity production rates are achievable using this interface to a μFFE device.

The intraday reproducibility of this two dimensional separation scheme was also determined using the same amino acid sample. Figure 3.6 shows 3 replicate two dimensional separations performed consecutively. Visual

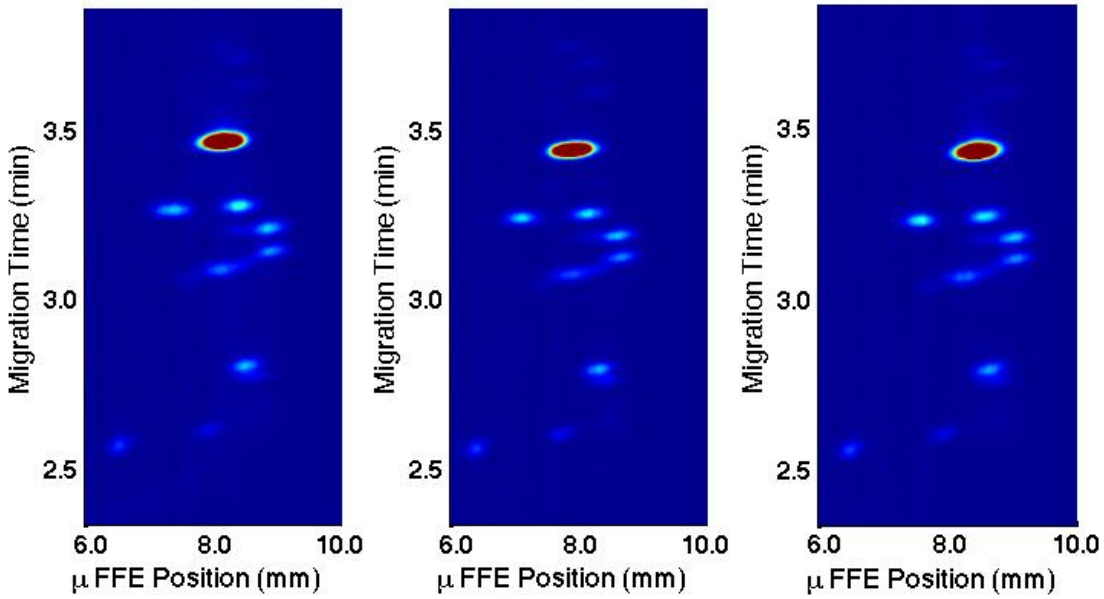

Figure 3.6. Contour plots of three replicate two dimensional capillary electrophoresis – μFFE separations of 13 amino acids labeled with AlexaFluor 488 (16 components). Close-up view for clarity. Separation conditions identical to Figure 3.5.

inspection of the contour plots indicates that under these separation conditions a reproducible pattern, or "fingerprint", has been achieved. Four arbitrarily selected peaks (1, 2, 11, and 16 in Fig 3.5 above) were used to calculate reproducibility in migration time, μFFE position, and peak height. Migration times (average and RSD for n = 3) were 2.56 min (0.23% RSD), 2.61 min (0.22% RSD), 3.25 min (0.63% RSD), and 3.74 min (0.36% RSD), for peaks 1, 2, 11, and 16, respectively. Peak positions in the μFFE separation dimension (average and RSD for n = 3) were 6.39 mm (1.08% RSD), 7.84 mm (0.87% RSD), 7.37 mm (1.92% RSD), and 8.28 mm (1.07% RSD), for peaks 1, 2, 11, and 16,

respectively. Peak heights (average and RSD for n = 3, in arbitrary units) were 12,431 (1.45% RSD), 7,929 (4.70% RSD), 22,558 (6.32% RSD), and 4,336 (5.50% RSD), for peaks 1, 2, 11, and 16, respectively.

The reproducibility metrics calculated above are encouraging since they give insight into individual parts of the two dimensional scheme. The excellent migration time reproducibility indicates that the homebuilt capillary electrophoresis separation is functioning as expected and can be counted on to give reproducible first dimension separations. The low peak height RSD indicates that the electrokinetic injection scheme employed can be done in a reproducible fashion. Finally, the low RSD in μFFE peak position indicates that flow in the device is stable, likely due to the presence of SDS (as discussed in Chapter 2).

3.5 Conclusions

An interface between capillaries and glass μFFE devices has been developed that minimizes dead volume and allows for efficient transfer of sample bands across the interface. This interface utilizes an etched capillary insertion channel, which places the outlet of the capillary in the separation chamber of the μFFE device. This interface was then used in a two dimensional separation scheme employing a homebuilt capillary electrophoresis first dimension separation and a μFFE second dimension separation. This scheme produced an

unadjusted peak capacity of 900 in less than 4 minutes and all 16 components of the sample mixture were resolved without previous optimization of the separation conditions. The adjusted peak capacity of 30 indicates that other separation modes should be explored to maximize the fractional coverage of the two dimensional space.

Note: this interface has since been used in another work by Geiger, Frost, and Bowser to couple nano liquid chromatography to a μFFE device with incredible results.[149]

Chapter 4

Fabrication and Operation of a Microchip Electrophoresis – Micro Free Flow Electrophoresis Device

4.1 Summary

While significant effort has been focused on developing an interface between a capillary and a μFFE device as detailed in Chapter 3, the need for seamless, reproducible integration of a first dimension separation with a μFFE device still exists. A microchip electrophoresis-micro free flow electrophoresis (ME-μFFE) device has been designed and fabricated in glass. By fabricating the first dimension separation channel and the μFFE separation channel in the same substrate, the dead volume that arises in the connections discussed in Chapter 3 is eliminated. In theory, these interfaces should be entirely reproducible because there effectiveness depends only on proper device fabrication.

Operation of this device using a reproducible electrokinetic gating injection scheme has been demonstrated and a loss in separation performance upon transfer of sample across the fabricated interface has been found to be essentially nonexistent. The performance of the first dimension electrophoretic separation was lower than expected and some suggestions for improving the performance are given.

4.2 Introduction

The advantage of a fabricated interface in a single substrate is fairly straightforward. The success of the interface depends only on the quality of the fabrication, not on the ability of the user to insert and bond a capillary into an etched channel in a reproducible fashion. So ultimately, the success of this integration of the separation dimensions depends on two main factors: the ability to etch relatively long defect-free channels in glass and the ability to perform small, reproducible sample injections.

The most cost-effective and convenient method for deep etching of channels in glass substrates is to use concentrated hydrofluoric acid (HF, 49%) and a robust masking material. This process, known as wet etching, produces etch rates much faster than any current dry etching technique. In order to etch defect-free channels in a glass substrate, the appropriate choice of masking material is essential. The masking material must stand up to prolonged exposure in concentrated HF but also be relatively easy to deposit and remove. Breakdown of the masking material can produce nonuniformities in channel edges, known as notch defects, or pinhole defects in areas that shouldn't be etched. A number of masking materials have shown the necessary resistance to concentrated HF including photoresists,[150,151] alternating layers of chromium (Cr) and gold (Au),[150-154] sputtered molybdenum,[155] amorphous silicon,[150,154,156,157] and polysilicon.[150,158] In this work, both Ti/Au masks and amorphous silicon

masks were used and evaluated (Section 4.4.1). It should be noted that the etching masks used in previous chapters did not necessarily provide defect-free etching but the feature size was large enough that defects did not affect device performance.

Another important, but often overlooked, consideration is the annealing of glass substrates prior to mask deposition. Glass substrates that have residual internal stresses from the manufacturing and polishing process can yield areas of varying etch rate and ultimately nonuniformities in the etched features.[157] In this work, through proper annealing and mask selection, defect-free channels were fabricated in borosilicate glass substrates.

An effective microchip electrophoresis device requires an injection scheme that yields reproducible injections of minute volumes of sample. A number of approaches, both hydrodynamic and electrokinetic in nature, have been developed since the inception of microchip electrophoresis for performing these injections.[159,160] However, the majority of injection schemes used in microchip electrophoresis are electrokinetic in nature due to the relative ease of controlling fluid flow in microfluidic devices by manipulating the applied potential at various buffer, sample, and waste reservoirs. For this reason, hydrodynamic injections will not be discussed further.

Some of the first electrokinetic-based injections on microfluidic devices were published in four reports in 1994 by Jacobsen *et. al*. The authors detailed a pinched injection mode,[161,162] a floating injection mode,[161] and a gated injection

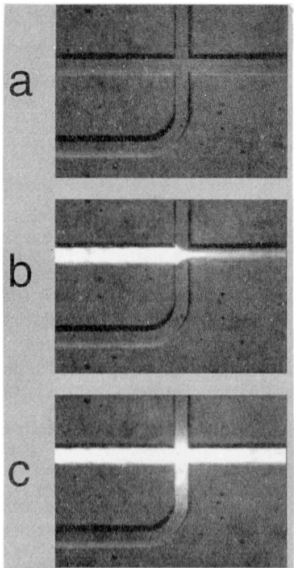

Figure 4.1. Injection cross (a), pinched injection mode (b), and floating injection mode (c) adapted from ref. 161. In the pinched injection in b, the sample width is time independent. In the floating injection in c, the sample width is diffusion controlled, and thus, time dependent.

mode[163,164] in a simple cross design shown in Figure 4.1a. In a pinched injection, sample is electrokinetically driven across the cross interface to waste by applying a positive potential to the sample reservoir while the waste reservoir is at ground. A positive potential is also applied to the two other reservoirs causing net fluid flow from these channels to waste as well. The result is a sample plug that has a defined width (based on the applied potentials) and is time independent. Applied potentials are then manipulated so the sample plug is carried down the separation channel by buffer. A pinched injection is shown in Figure 4.1b. In a floating injection, sample is electrokinetically driven across the cross interface to waste just as in the pinched injection mode. However, the two other reservoirs are allowed to “float” so there is no “pinching” of the sample stream. The result is

a sample plug width that is diffusion controlled and thus is time dependent. Again, the applied potentials are then manipulated so the sample plug is carried down the separation channel by buffer. A floating injection is shown in Figure 4.1c. The pinched injection mode is often preferred to the floating injection mode due to more precise control of the sample plug width. The downside of these injection modes is that fluid flow in the separation channel is either halted (floating injection mode) or reversed (pinched injection mode) making either not a great choice for a two dimensional separation scheme where continuous flow in the first dimension is preferred, and often necessary. In a gated injection scheme, a positive potential is applied to both the buffer and sample reservoirs while the waste and the end of the separation channel are held at ground. If the electroosmotic flow velocity of the buffer stream is larger in magnitude than that of the sample stream as they approach the cross interface, the sample stream will be “gated” to waste by the buffer stream and only the buffer stream will enter the separation channel. This is commonly referred to as the separation mode. To perform an injection, the buffer and waste reservoirs are “floated” for a set period of time allowing the sample stream to enter the cross interface and potentially the separation channel. The potentials at the reservoirs are then returned to their separation mode configuration and the sample stream is again gated to waste by the buffer stream. The resulting sample plug width is dependent on the electroosmotic flow velocity of the sample stream in the “floating” voltage configuration and the time spent in the “floating” voltage configuration. An

example of a gated injection sequence is shown later in this work in Section 4.4.2.

All the injection modes discussed so far have been implemented in a cross design, which is common, but it should be noted that variations of these injections have also been used in other channel geometries such as a T design,[165-167] a cross-T design,[168,169] and a multi-T design.[170,171] An extensive review on electrokinetic-based injection schemes with various channel geometries can be found in the literature.[159] Electrokinetically gated injections are most compatible with two dimensional separation schemes as fluid flow through the first dimension is continuous, or in other words, there are not periods during the injection sequence where flow in the separation channel is halted or reversed as in the other injection modes. A simple cross design with electrokinetically gated injections was chosen for this work.

In this work, a microchip electrophoresis-micro free flow electrophoresis device utilizing an electrokinetically gated sample injection scheme has been fabricated in an all glass device. The operation of this device has been demonstrated and its future use in two dimensional separations is discussed.

4.3 Experimental

4.3.1 Chemicals and Reagents

Deionized water (18.3 MΩ, Millipore, Billerica, MA) was used for all buffer and sample preparations. CAPS was obtained from Alfa Aesar (Heysham, Lancashire, UK) in 98% purity. Triton X-100 was obtained from Sigma-Aldrich. Buffers were adjusted to appropriate pH by addition of 50% NaOH obtained from Sigma-Aldrich. Aqueous buffers were vacuum filtered through a 0.22 µm nitrocellulose membrane filter (Fisher Scientific, Fairlawn, NJ) before use. The microchip electrophoresis and µFFE run buffer consisted of 20 mM CAPS adjusted to pH 10.00 with 50% NaOH with 300 µM Triton X-100 (Sigma-Aldrich). Disodium fluorescein (Acros Organics, NJ) and Rhodamine 110 (Sigma-Aldrich) were prepared in 190 proof ethanol (Fisher Scientific) and diluted in separation buffer to concentrations of 1.0 mM. Piranha solutions (4:1 H_2SO_4/H_2O_2)(Ashland Chemical, Dublin, OH) were used to clean glass wafers and etch unwanted Ti. GE-6 (Acton Technologies, Inc., Pittston, PA) was used to etch unwanted Au. Concentrated HF (49%)(Ashland Chemical) was used to etch the glass wafers. Silver conductive epoxy (MG Chemicals, Surrey, BC, Canada) was used to make electrical connections to the µFFE device. Corning® cloning cylinders (Sigma-Aldrich) were used as buffer and waste reservoirs. Super glue (3M, St. Paul, MN) was used to fix buffer and waste reservoirs to the device.

4.3.2 Device Fabrication

A multiple depth ME-μFFE device was fabricated similar to a previously described fabrication scheme,[59] with a few major changes. First, a 1.1 mm borofloat glass wafer (Precision Glass & Optics, Santa Ana, CA) was annealed in an oven at 560°C for 6 hours and allowed to cool to room temperature slowly by not opening the oven door. An amorphous silicon masking layer was then deposited by PECVD for 3 hours per side resulting in a film thickness of ~800 nm. The substrate and mask were then annealed in an oven at 400°C for 4 hours and allowed to cool to room temperature slowly overnight. Then, 62 μm deep electrode channels were etched into the wafer using standard photolithography procedures. A second photolithography procedure defined the μFFE separation channel and the first dimension electrophoresis channel and injection cross, leaving a 22 μm deep by 1 cm wide by 2.5 cm long separation channel, 22 μm deep by 54 μm wide by 20 cm long electrophoresis channel and injection cross, and 84 μm deep electrode channels. The featured wafer was then masked with cleanroom tape to prevent metal deposition in the electrophoresis channel and injection cross. A 150 nm thick layer of Ti was then deposited by a Temescal electron beam evaporator, followed by a 150 nm thick layer of Au. The cleanroom tape was then removed and a final photolithography and etching procedure was used to remove the unwanted Ti and Au to define the electrodes. Access holes were then drilled into the featured wafer at the end of each injection cross channel for connection to buffer reservoirs using a 1 mm

diameter diamond tip drill bit (Lasco Diamond Products, Chatsworth, CA) and a Dremel tool. A second wafer with pre-drilled 1 mm access holes and a ~90 nm thick layer of amorphous silicon (aSi) was aligned with the featured wafer and anodically bonded (900 V, 3 h, 450 ºC, 5 mbar) using a Karl Suss SB-6 wafer bonder (Munich, Germany). Nanoports (IDEX, Oak Harbor, WA) were attached over µFFE access holes for fluidic connections. Silver conductive epoxy was used to attach lead wires to the electrodes. The µFFE region was perfused with 1M NaOH to remove aSi from the channels. The electrophoresis channel and injection cross were cleared of unwanted aSi by filling buffer reservoirs with 1M NaOH and applying a vacuum at a µFFE outlet with the other outlets and inlets sealed. A completed device is shown below in Figure 4.2.

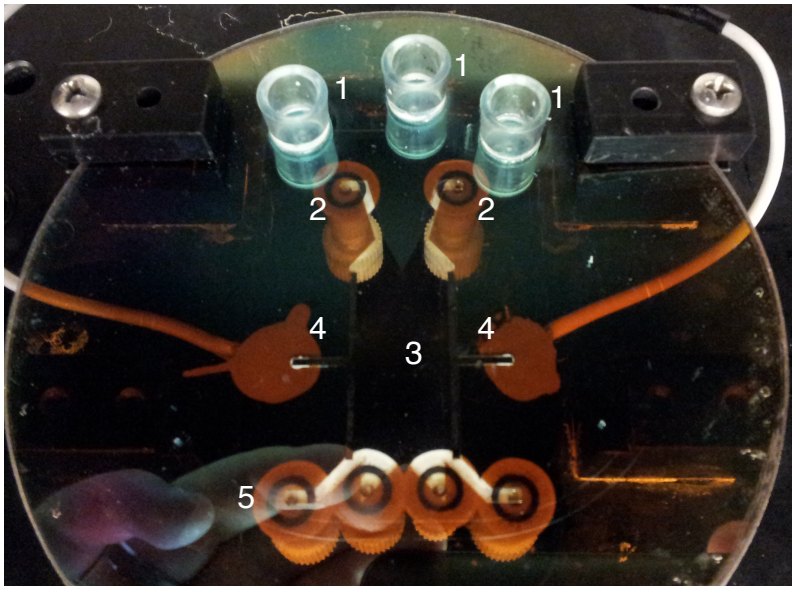

Figure 4.2. An example of a microchip electrophoresis-micro free flow electrophoresis (ME-µFFE) device. ME buffer, sample, and waste reservoirs (1), µFFE buffer inlets (2), µFFE separation chamber (3), µFFE electrodes (4), µFFE buffer outlets (5).

4.3.3 Device Operation

Spellman CZE1000R power supplies were used to apply potentials to reservoirs using platinum wire electrodes. Kilovac SO5LTA345 high voltage relays were used to quickly manipulate voltages at each reservoir. The power supplies and relays were controlled using a BNC 2110 DAQ board (National

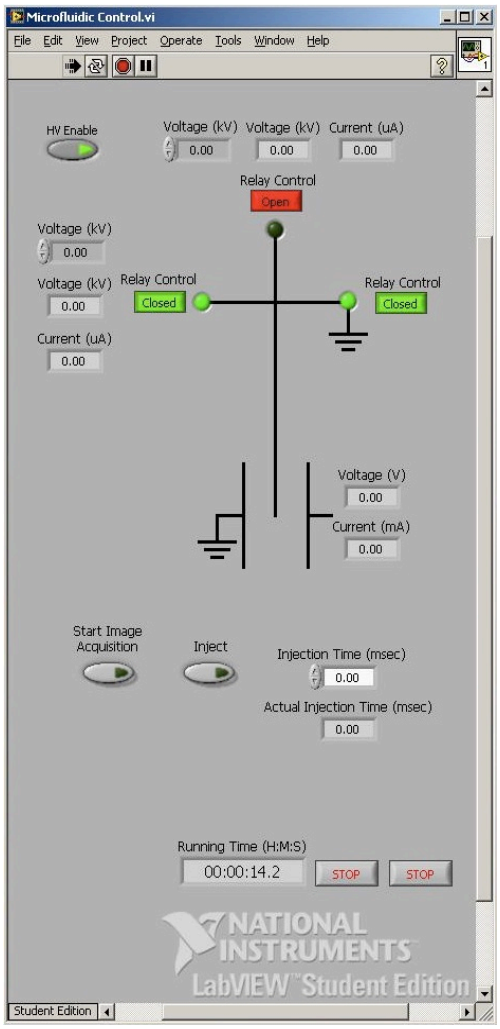

Figure 4.3. LabVIEW interface for controlling a microchip electrophoresis-micro free flow electrophoresis device (ME-μFFE). The interface includes individual controls for enabling the high voltage supplies, setting the potentials of the supplies, monitoring the potential applied and current applied, turning relays on/off, monitoring μFFE voltage and current, arming image acquisition, and performing gated sample injections for a given injection time.

Instruments, Austin, TX), PCIe-6321 DAQ card (National Instruments, Austin, TX), isolated from the high voltage components by optocouplers. All device operations can be performed from a single LabVIEW interface (Figure 4.3) including manipulating the power supplies, manipulating the high voltage relays to perform sample injections, and triggering image acquisition.

4.3.4 Data Collection and Processing

The μFFE separation channel and electrophoresis injection cross were imaged using a QuantEM:512SC CCD camera (Photometrics, Tucson, AZ) attached to a SMZ1500 stereomicroscope (Nikon Corp., Tokyo, Japan) with a 1.6x objective lens. The microscope was equipped with an Endow GFP bandpass emission filter cube (Nikon Corp.) containing two bandpass filters (450-490 and 500-550 nm) and a dichroic mirror with a 495 nm cutoff. Laser induced fluorescence (LIF) detection was performed using a 150 mW, Argon-ion laser (Melles Griot, Carlsbad, CA) expanded into a ~2.5 cm x ~150 μm line across the separation channel or the injection cross. The entire instrument setup was enclosed in black, rubberized fabric (Thorlabs, Newton, NJ) to minimize stray light. MetaVue software was used for imaging. The exposure time was 100 milliseconds to balance signal strength and acquisition rate. Images were processed using an in-house MATLAB routine.

4.4 Results and Discussion

4.4.1 Fabrication of Defect-Free Channels

The traditional device fabrication scheme used to make devices in Chapter 2 and 3 (pictured in Figure 1.2) was not sufficient to produce long defect-free electrophoresis channels in glass. The traditional fabrication scheme used in those chapters is susceptible to "pinhole" defects on the glass surface due to the aggressive HF etchant compromising the amorphous silicon masking layer. These "pinhole" defects did not adversely affect device performance because the feature size was generally much larger than the size of the defects. For this reason, improvements to the traditional fabrication scheme were not explored. In order to etch long defect-free channels in glass, however, other masking materials and/or procedures were explored since even a single "pinhole" defect can have drastic effects on separation performance.

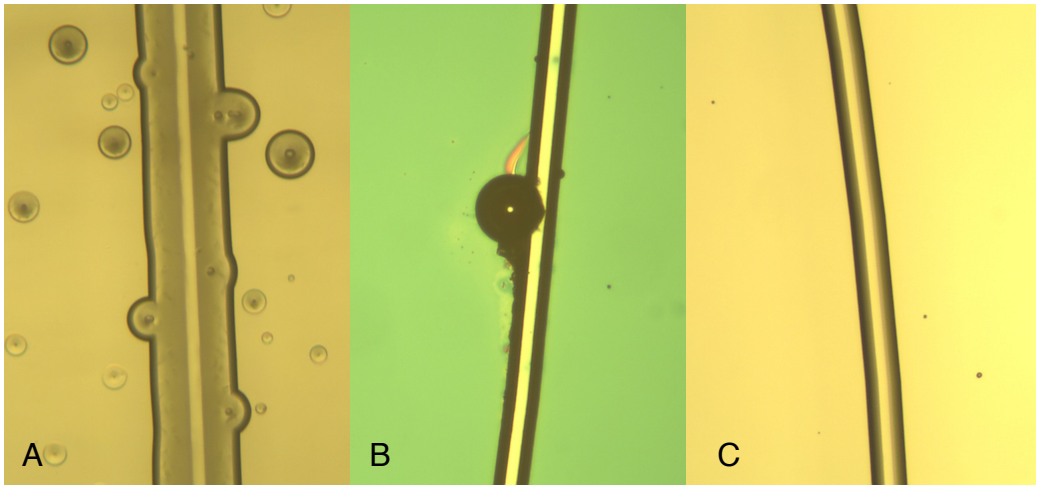

Figure 4.4. Electrophoresis channels in borosilicate glass after HF etching with a ~750 nm Ti/Au masking layer (A), a ~540 nm amorphous silicon masking layer annealed at 400°C for 2 hours (B), and a ~800 nm amorphous silicon masking layer annealed at 400°C for 6 hours (C).

As mentioned in the introduction, numerous masking materials have been shown to withstand periods of prolonged HF exposure including Cr/Au and amorphous silicon. Figure 4.4A shows a magnified view of an etched channel in borosilicate glass using a 100 nm Ti/650 nm Au masking layer. It is clear that there is an excessive number of "pinhole" defects over the entirety of the surface and that a uniformly etched channel is just not possible with this masking layer. Figure 4.4B shows an etched channel using a 540 nm amorphous silicon masking layer that has been annealed at 400°C for 2 hours. This masking material and procedure is the same as in the traditional fabrication scheme mentioned in the previous paragraph. The number of "pinhole" defects is reduced as compared to Figure 4.4A but the prevalence of these defects is still significant. It is clear that the channel shown in Figure 4.4B will not yield the separation performance needed. There is evidence to suggest that the cause of these defects is due to residual stress in the amorphous silicon masking layer from the deposition process.[157] Longer annealing times have been shown to remove residual stress in PECVD amorphous silicon layers.[157] Figure 4.4C shows an etched channel using an 800 nm amorphous silicon masking layer that has been annealed at 400°C for 6 hours. It is clear that a combination of a thicker amorphous silicon masking layer (540 vs 800 nm) and longer annealing time (2 vs 6 hours) produces a mask that is more resistant to HF. The channel was completely defect-free over its entire 20 cm length.

Even with an improved masking procedure, occasional channel defects still occurred that were not consistent with mask failure. An example of these defects are shown in Figure 4.5A. It is apparent that there were regions of the glass substrate that would preferentially etch more rapidly than others causing erratic etching patterns. The manufacturing process of borosilicate glass substrates is known to leave internal residual stresses in the material that can give rise to uneven etching rates.[157] Annealing these glass substrates prior to any processing can relieve these internal stresses and yield consistent etch rates over the entire substrate surface.[157] Figure 4.5B shows an etched injection cross after annealing of the glass substrate at 560°C for 6 hours and the successful masking procedure discussed above. All instances of "pinhole" defects and preferential etching are absent. This procedure of annealing glass substrates prior to masking has been adopted for all devices in this chapter.

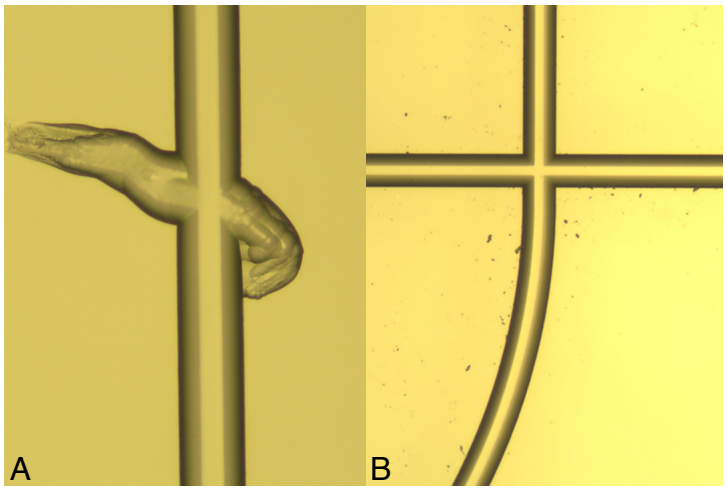

Figure 4.5. Electrophoresis channels in borosilicate glass after HF etching with a a ~800 nm amorphous silicon masking layer annealed at 400°C for 6 hours with no annealing of the glass substrate prior to masking (A) and with annealing at 560°C for 6 hours prior to masking (B).

4.4.2 Injection Sequence

Figure 4.6A shows the injection cross under separation mode conditions. Separation mode consists of a 10 kV potential at the buffer reservoir (top), a 7 kV potential at the sample reservoir (right), and the waste reservoir (bottom) and electrophoresis channel (left) held at ground. The sample stream is effectively gated to waste under this voltage configuration, as no fluorescent signal is detectable in the electrophoresis channel. Figure 4.6B shows the injection cross after switching to injection mode where the buffer reservoir (top) and waste reservoir (bottom) are "floated". The sample stream begins to enter the electrophoresis channel. Figure 4.6C shows the injection cross after switching back to separation mode. The sample stream is again gated to waste and a small volume of sample has been injected into the electrophoresis channel. Replicate injections were performed to assess the reproducibility of this injection scheme.

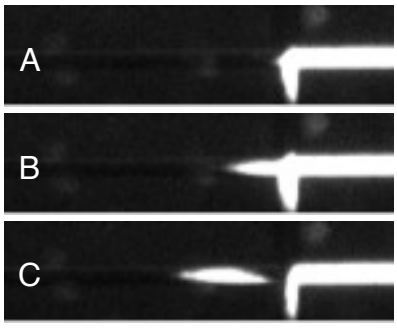

Figure 4.6. Injection cross under separation mode (A), injection mode (B), and returning to separation mode (C). In separation mode, 10 kV is applied to the buffer reservoir (top), 7 kV is applied to the sample reservoir (right), and the waste reservoir (bottom) and electrophoresis channel (left) are held at ground. In injection mode, the buffer reservoir (top) and waste reservoir (bottom) are "floated" while the sample reservoir (right) remains at 7 kV and the electrophoresis channel remains grounded.

Injection reproducibility is essential to quantitative electrophoretic separations. To assess the reproducibility of this gated injection scheme, 20 replicate injections of Rhodamine 110 at four injection times (50, 100, 200, 400 msec) were performed simultaneously as shown in Figure 4.7. All injections were performed in less than 2 minutes to minimize any drift in electroosmotic flow velocity, which is directly related to the injection volume. The average peak areas (in arbitrary units) of Rhodamine 110 (n = 20) at 50, 100, 200, and 400 millisecond injection times were 2,653 (17.1% RSD), 3,890 (16.0% RSD), 6,276 (13.9% RSD), and 9,723 (10.2% RSD), respectively. Despite the rather large relative standard deviations when compared to electrokinetic injections performed in automated capillary electrophoresis instruments (1.5% - 6.5% RSD)[172], this data is encouraging for a number of reasons. First, the data sampling rate was not fast enough to take a sufficient number of data points

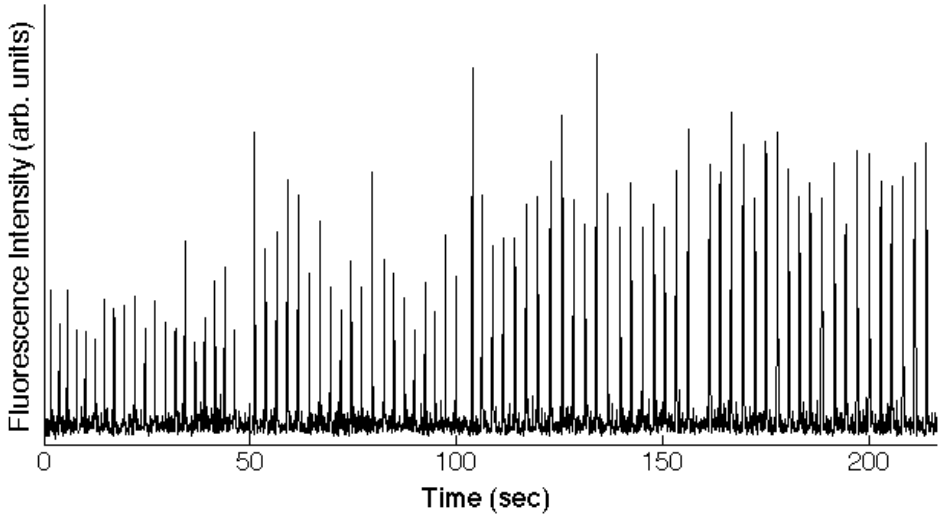

Figure 4.7. Twenty replicate injections of Rhodamine 110 at injection times of 50, 100, 200, and 400 milliseconds (groups of 20, left to right). Detection was performed immediately after the injection cross at 10 Hz.

across a full peak width. In fact, for the 50 ms injections, only two to three data points were recorded above baseline. This makes assessment of peak area difficult and unreliable, or in other words, it is likely that the true volume injected is more reproducible than the relative standard deviations suggest. Second, the relative standard deviations are actually impressive considering the extremely short injection times relative to capillary electrophoresis instruments (msec vs sec). If the electroosmotic flow velocity of the buffer and sample streams were significantly reduced by lowering the applied potentials at the reservoirs, longer injection times could be employed which would certainly improve the injection reproducibility. The potentials at the reservoirs could then be increased after sample injection to increase the electric field strength in the separation channel. The decrease in relative standard deviation with increased injection time shown in the data above supports this idea. Third, the average peak areas increase linearly (R^2 = 0.992) with injection time indicating that the gated injection scheme is functioning as expected (Figure 4.8).

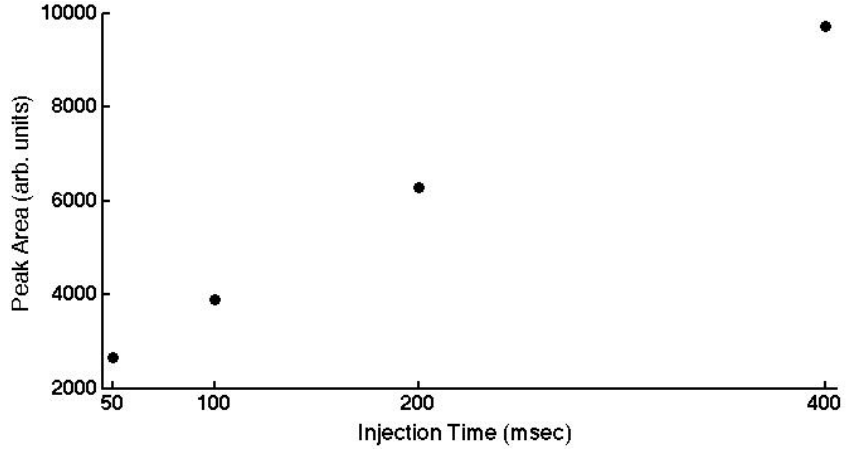

Figure 4.8. Peak area versus injection time using the electrokinetic injection scheme detailed in Section 4.4.2.

4.4.3 Interface Assessment

To test the quality of the fabricated interface, the 4σ peak width of Rhodamine 110 immediately before entering the μFFE separation space was compared to the 4σ peak width immediately after entering the μFFE separation space (Figure 4.9). This process is the same as how interfaces were evaluated in Chapter 3. From Figure 4.9, it is clear that this fabricated interface does not cause peak broadening upon transfer from electrophoresis channel to μFFE separation channel. The 4σ width of the Rhodamine 110 peak immediately before entering the μFFE separation space, averaged from 5 replicate injections, was 1.674 seconds (0.45% RSD). The average 4σ width (n = 5) of the Rhodamine 110 peak immediately after entering the μFFE separation space was 1.675 seconds (2.9% RSD). Statistically speaking, there is no observable

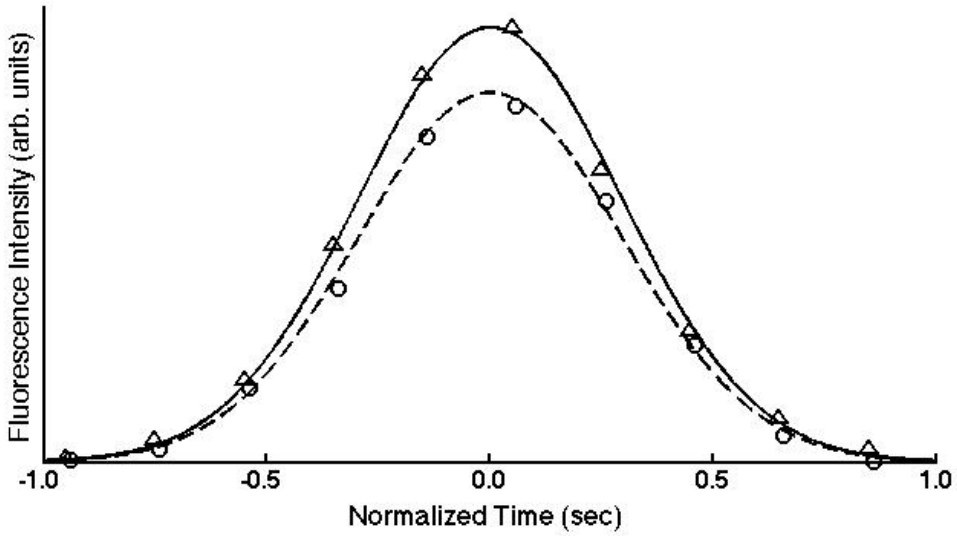

Figure 4.9. Comparison of Rhodamine 110 peaks immediately before entering the μFFE separation space (triangles with solid line) and immediately after entering the μFFE separation space (circles with dashed line). Curves are Gaussian fits to the experimental data shown. Time has been normalized for ease of comparison.

broadening of the Rhodamine 110 upon transfer from the electrophoresis channel to the μFFE separation space. This finding corroborates the initial idea that an interface entirely fabricated in glass should not be subject to the potential dead volumes in capillary-device interfaces discussed in Chapter 3. Using this device, the focus can now turn to maximizing separation performance in each dimension, developing orthogonal separation mechanisms, and ultimately maximizing two dimensional peak capacities. The effectiveness of the interface between dimensions is no longer a concern.

4.4.4 Efficiency of First Dimension Separation

While this device has been shown to be capable of reproducible electrokinetic injections and efficient transfer of sample between separation dimensions, the performance of the first dimension electrophoretic separation was quite poor.

Figure 4.10 shows a comparison of peak widths of Rhodamine 110 immediately after injection (triangles with solid line) and immediately before transfer to the μFFE separation space (circles with dotted line). Also included in Figure 4.10 is a simulated peak for Rhodamine 110 if only longitudinal diffusion broadening is considered (dashed line) using a diffusion coefficient for Rhodamine 110 of 4.4×10^{-6} cm^2/sec (Gendron *et. al.*[173]) and a time of 77.2 seconds (the actual average migration time of Rhodamine 110 in this comparison).

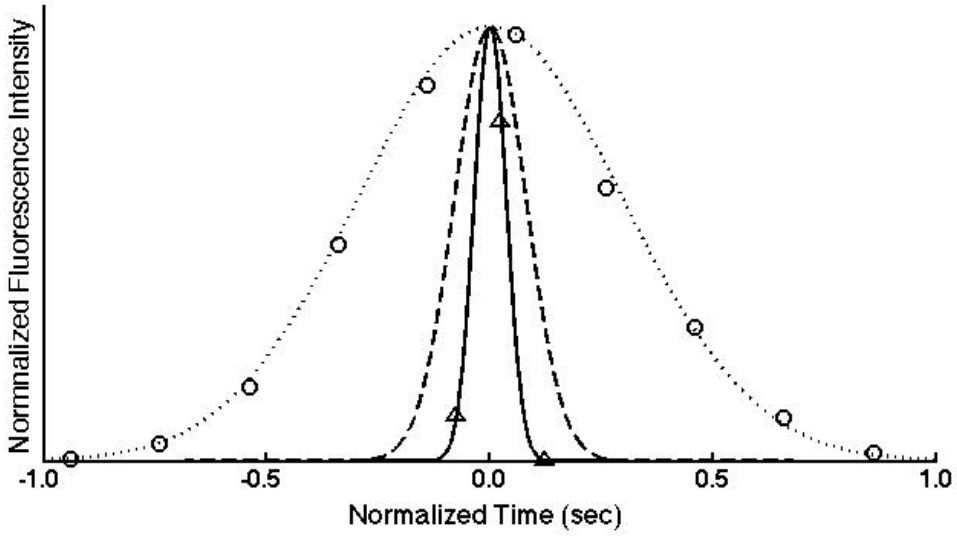

Figure 4.10. Comparison of Rhodamine 110 peaks immediately after sample injection (triangles with solid line), immediately before entering the μFFE separation space (circles with dotted line), and a simulated peak if longitudinal diffusion was the only contributing factor to peak broadening (dashed line). Curves are Gaussian fits to the experimental data shown (except simulated peak). Time and fluorescence intensity have been normalized for ease of comparison.

It is clear that longitudinal diffusion is not the only cause of peak broadening as was generally expected when designing this device. In fact, longitudinal diffusion broadening only accounts for roughly 6% of the observed peak variance after 77.2 seconds of migration time. It is possible that small defects still exist in the ~20 cm long electrophoresis channel which could perturb the electroosmotic flow profile and ultimately yield broader peaks than expected. However, visual inspection of the entire electrophoresis channel under microscope did not provide evidence that this is the case. It is also possible that adsorption of Rhodamine 110 to the walls of the electrophoresis channel is contributing to the broadening of the peak. Years of experience performing

electrophoresis with this dye suggest that adsorption is not contributing significantly to peak broadening. It is more likely that we are not operating under true “plug flow” conditions. The electroosmotic “plug flow” profile is only achievable under conditions where the channel, or capillary, has no net pressure drop from inlet to outlet. In the monolithic device described here, the electroosmotic flow from the first dimension is flowing against a positive pressure in the device (a consequence of pressure driven flow in the μFFE portion of the device). Numerous models have shown that electroosmotic flow profiles will have an inverted parabolic shape in the face of positive backpressure.[174,175] This can lead to significant Taylor-Aris dispersion, or hydrodynamic dispersion, causing bands to broaden considerably more than is expected under “plug flow” conditions. More data would be required to quantify whether this is the case. If this is the cause of the relatively poor performance of the first dimension separation in the device, developing a scheme to pressurize the reservoirs to eliminate any pressure differences from the reservoirs to the μFFE portion of the device should give rise to true “plug flow” conditions and efficient first dimension separations.

4.5 Conclusions

A microchip electrophoresis-micro free flow electrophoresis device has been fabricated in borosilicate glass. A system of power supplies and high voltage relays has been constructed to perform sufficiently reproducible

electrokinetic injections. The fabricated interface between separation dimensions has been shown to not contribute to peak broadening. The backpressure in the μFFE separation channel appears to be limiting the separation performance of the first dimension microchip electrophoresis separation. If first dimension separation performance can be maximized, this device certainly has the capability of performing fast two dimensional separations (high peak capacity production rates).

Acknowledgments

Thank you to Edgar Arriaga for generously loaning a power supply and high voltage relays to support this work.

Chapter 5

Summary and Future Outlook

5.1 Summary

Micro free flow electrophoresis is a separation technique which is well suited for long-term continuous monitoring applications and as a second dimension separation technique in a two dimensional scheme due to its continuous nature. Separations are performed in space, rather than time, so discrete sample injections are not required. This work pointed out two areas of development that were necessary for micro free flow electrophoresis to be able to offer its continuous separation advantages; improving the stability of separated analyte streams and being able to interface μFFE devices to the "outside world" in a zero dead volume manner. This work has addressed these areas of improvement and has given some highlights for the future of this technique.

In Chapter 2, the stability of separated analyte streams was improved by use of two classes of buffer additives, surfactants and nonaqueous solvents. We hypothesize that the addition of surfactant or nonaqueous solvent promotes the formation of smaller electrolysis bubbles by lowering the surface tension, making it easier for these bubbles to be cleared from the device. The addition of the surfactants Triton X-100 and sodium dodecyl sulfate (SDS) were shown to improve the stability of separated streams of fluorescent dyes by 12-fold and 6-fold, respectively. Triton X-100 proved to be a better additive due to its nonionic nature (its addition doesn't increase conductivity). The addition of the nonaqueous solvents methanol and acetonitrile also were shown to improve the

stability of separated streams of fluorescent dyes by 8-fold and 6-fold, respectively. The impact of this work was summed up by performing the longest, continuously stable, μFFE separation to date. Three fluorescent dyes were separated and their position was held stable for nearly two hours, a 6-fold improvement over any published works to date.

In Chapter 3, a new interface has been developed allowing for zero dead volume coupling of a capillary to an all glass μFFE device. This interface centers on the fabrication of a capillary insertion channel, which allows the capillary outlet to rest in the μFFE separation chamber. This was done by adding a third photolithography step during device fabrication to allow for the wet etching of this capillary insertion channel. The capillary was then inserted into this channel and fixed with a heat sensitive adhesive. Monitoring the extent of broadening as peaks travelled across the interface allowed for quantitative assessment of the effectiveness of this interface. Statistically speaking, there was no observable broadening of peaks upon transfer from capillary to μFFE device across the interface. The effectiveness of this interface was then demonstrated in the first two dimensional separation using μFFE as the second dimension separation technique. A 16-component mixture of fluorescently labeled amino acids was resolved in less than four minutes using a homebuilt capillary electrophoresis – micro free flow electrophoresis two dimensional separation scheme. This is especially impressive considering there was no optimization of the separation

conditions, highlighting the power of high peak capacity separations for relatively simple sample mixtures.

In Chapter 4, a microchip electrophoresis – micro free flow electrophoresis device was designed and fabricated allowing for seamless integration of two separation techniques. This integrated device provided a true zero dead volume interface between the separation dimensions since the entire device is fabricated in the same substrate, ultimately eliminating any “human component” to the effectiveness of the interface. Several changes to the typical fabrication scheme were developed to allow the fabrication of this device including annealing the substrates prior to fabrication and a new masking procedure. Defect free devices were fabricated using these new techniques. An electrokinetic gating scheme for sample injection was developed using this integrated device using high voltage relays to quickly manipulate the applied potential at buffer, sample, and waste reservoirs. The effectiveness of this entirely fabricated interface was assessed by monitoring the extent of peak broadening across the interface. There was no observable broadening of peaks across the interface.

5.2 Future Outlook

Significant progress has been made in realizing the power of micro free flow electrophoresis as a second dimension separation technique in a two dimensional separation scheme. This work has pointed out, however, that

orthogonal separation mechanisms must still be developed to maximize the fractional coverage of the two dimensional separation space and ultimately maximize the actual two dimensional peak capacity that can be achieved (it should be noted that labeling with AlexaFluor 488 likely reduced the dimensionality of the sample as well). This can be done in two ways: either by combining various electrophoretic separation modes that exploit different chemical properties for separation (such as CZE, MEKC, or IEF) or by interfacing micro free flow electrophoresis with a non-electrophoretic based separation technique (such as nano liquid chromatography). It should be noted that coupling nano liquid chromatography and micro free flow electrophoresis has already been utilized with great success,[149] but the numerous possibilities for combinations of separation modes still exist. If electrophoretic modes can be found that are orthogonal, the homebuilt capillary electrophoresis – micro free flow electrophoresis instrument described in Chapter 3 and the microchip electrophoresis – micro free flow electrophoresis device described in Chapter 4 should provide large actual peak capacities in rather short amounts of time (high actual peak capacity production rates). It would be nice to see these techniques then utilized for real-life applications, such as proteomic "fingerprinting" of tissues as has been shown in the literature on two dimensional capillary electrophoresis schemes.[176] In terms of applications, long term continuous monitoring of neurotransmitters from rat brain or cell models remains an interest of our group and the advances made in this work in terms of zero dead volume connections to

μFFE devices should open the door for these types of experiments to be realized. The technology is now in place for μFFE devices to make their way into our neuroscience labs and offer sampling rates on the hundreds of milliseconds scale as opposed to the tens of seconds scale that is currently being used.

While significant advancements in μFFE device design, fabrication, and operation have been made in this work, two other areas of improvement still exist: analyte detection schemes and alternative device materials. Laser induced fluorescence detection has been employed in this work (and all of the group's work) due to its high sensitivity and its ability to perform detection in space when coupled with a CCD camera. Ultimately, there are many samples that may not be easily fluorescently labeled and may need alternate detection schemes such as UV or electrochemical-based methods. These detection methods have been utilized in microchip electrophoresis and may be amenable to μFFE devices, however, the short pathlength and spatial nature of detection may make this challenging. Mass spectrometry detection may prove to be the most useful (and powerful) if a proper technique for coupling μFFE devices to mass spectrometers can be developed. Conventional separation techniques (GC, HPLC, CE) have benefited greatly from mass spectrometric detection (or tandem mass spectrometric detection) and the ability to couple μFFE devices to this type of detection should reap incredible benefits, mainly the ability to get qualitative information about sample components.

The other existing drawback is the relatively high cost and low production speed of all glass μFFE devices. If this technology is ever to be commercialized in any form, other device materials and fabrication schemes that are cheaper and faster must be developed. Rigid polymeric materials, such as poly(methyl methacrylate) (PMMA), that can be hot embossed are an intriguing possibility for μFFE devices. This allows many devices to be fabricated from a single master template. Also, recent advancements in three dimensional printing using polylactide (PLA) could allow for fabrication of a device from a commercially available 3D printer. Both are realistic options for future μFFE devices and should be explored.

Micro free flow electrophoresis (μFFE) has come a long way in the past 20 years but is still in its infancy. The μFFE devices, fabrication schemes, and methods I started working on only partially resemble the types of devices and fabrication schemes the group uses today. I feel grateful that I was able to contribute to the growth of μFFE as a viable separation technique and look forward to see where it goes in the future.

Bibliography

(1) Whitesides, G. M. *Nature* **2006**, *442*, 368.
(2) Bente III, P. F.; Zerenner, E. H.; Dandeneau, R. D.; Hewlett-Packard Company (Palo Alto, CA): United States, 1981.
(3) Dandeneau, R. D.; Bente III, P. F.; Rooney, T.; Hiskes, R. *American Laboratory* **1979**, *11*, 61.
(4) Dandeneau, R. D.; Bente III, P. F.; Rooney, T.; Hiskes, R. *International Laboratory* **1979**, 69.
(5) Premstaller, A.; Oberacher, H.; Huber, C. G. *Anal. Chem.* **2000**, *72*, 4386.
(6) Premstaller, A.; Oefner, P. J.; Oberacher, H.; Huber, C. G. *Anal. Chem.* **2002**, *74*, 4688.
(7) Dominguez-Vega, E.; Kotkowska, O.; Garcia, M. C.; Crego, A. L.; Marina, M. L. *J. Chromatogr. A* **2011**, *1218*, 4928.
(8) Chen, X.; Tolley, H. D.; Lee, M. L. *J. Chromatogr. A* **2010**, *1217*, 3844.
(9) Kuban, P.; Hauser, P. C. *J. Chromatogr. A* **2007**, *1176*, 185.
(10) Wei, H.; Nolkrantz, K.; Parkin, M. C.; Chisolm, C. N.; O'Callaghan, J. P.; Kennedy, R. T. *Anal. Chem.* **2006**, *78*, 4342.
(11) Deng, Q.; Kauri, L. M.; Qian, W. J.; Dahlgren, G. M.; Kennedy, R. T. *Analyst* **2003**, *128*, 1013.
(12) Skoog, D. A.; Holler, F. J.; Crouch, S. R. *Principles of Instrumental Analysis*; 6th ed.; Brooks/Cole: Thomson Learning: Australia, 2007.
(13) Frost, N. W.; Jing, M.; Bowser, M. T. *Anal. Chem.* **2010**, *82*, 4682.
(14) Kasicka, V. *Electrophoresis* **1999**, *20*, 3084.
(15) Zhang, Z.; Zhang, F.; Liu, Y. *Journal of Chromatographic Science* **2013**, *51*, 666.
(16) Terry, S. C.; Jerman, J. H.; Angell, J. B. *IEEE Transactions on Electron Devices* **1979**, *26*, 1880.
(17) Manz, A.; Graber, H. M.; Widmer, H. M. *Sensors and Actuators B* **1990**, *1*, 244.
(18) Manz, A.; Miyahara, Y.; Miura, J.; Watanabe, Y.; Miyagi, H.; Sato, K. *Sensors and Actuators B* **1990**, *1*, 249.
(19) Harrison, D. J.; Fan, Z. H.; Seiler, K.; Manz, A. *Analytica Chimica Acta* **1993**, *283*, 361.
(20) Harrison, D. J.; Manz, A.; Fan, Z. H.; Ludi, H.; Widmer, H. M. *Anal. Chem.* **1992**, *64*, 1926.
(21) Manz, A.; Harrison, D. J.; Verpoorte, E. M. J.; Fettinger, J. C.; Paulus, A.; Ludi, H.; Widmer, H. M. *J. Chromatogr.* **1992**, *593*, 253.
(22) Effenhauser, C. S.; Manz, A.; Widmer, H. M. *Anal. Chem.* **1993**, *65*, 2637.
(23) Hu, H. M.; Li, Z. H.; Zhang, X. N.; Xu, C. X.; Guo, Y. M. *J. Sep. Sci.* **2013**, *36*, 3419.
(24) Nii, K.; Sueyoshi, K.; Otsuka, K.; Takai, M. *Microfluidics and Nanofluidics* **2013**, *14*, 951.

(25) von Heeren, F.; Verpoorte, E.; Manz, A.; Thormann, W. *Anal. Chem.* **1996**, *68*, 2044.
(26) Jin, S.; Anderson, G. J.; Kennedy, R. T. *Anal. Chem.* **2013**, *85*, 6073.
(27) Walker, P. A.; Morris, M. D.; Burns, M. A.; Johnson, B. N. *Anal. Chem.* **1998**, *70*, 3766.
(28) Hofmann, O.; Che, D. P.; Cruickshank, K. A.; Muller, U. R. *Anal. Chem.* **1999**, *71*, 678.
(29) Mao, Q.; Pawliszyn, J. *Analyst* **1999**, *124*, 637.
(30) Yatsushiro, S.; Yamaguchi, Y.; Yamamura, S.; Shinohara, Y.; Baba, Y.; Kataoka, M. *J. Pharm. Bio. Anal.* **2011**, *55*, 202.
(31) Mohamadi, M. R.; Svobodova, Z.; Verpillot, R.; Esselmann, H.; Wiltfang, J.; Otto, M.; Taverna, M.; Bilkova, Z.; Viovy, J. L. *Anal. Chem.* **2010**, *82*, 7611.
(32) Colyer, C. L.; Mangru, S. D.; Harrison, D. J. *J. Chromatogr. A* **1997**, *781*, 271.
(33) Rodriguez, I.; Zhang, Y.; Lee, H. K.; Li, S. F. Y. *J. Chromatogr. A* **1997**, *781*, 287.
(34) Rodriguez, I.; Lee, H. K.; Li, S. F. Y. *Electrophoresis* **1999**, *20*, 118.
(35) Ramseier, A.; von Heeren, F.; Thormann, W. *Electrophoresis* **1998**, *19*, 2967.
(36) Duffy, C. F.; MacCraith, B.; Diamond, D.; O'Kennedy, R.; Arriaga, E. A. *Lab Chip* **2006**, *6*, 1007.
(37) Barrollier, J.; Watzke, E.; Gibian, H. *Z. Naturforschung* **1958**, *13B*, 754.
(38) Hannig, K. *Z. fuer Anal. Chem.* **1961**, *181*, 244.
(39) Hoffstetter-Kuhn, S.; Wagner, H. *Electrophoresis* **1990**, *11*, 451.
(40) Caslavska, I.; Gebauer, P.; Thormann, W. *J. Chromatogr.* **1991**, *585*, 145.
(41) Caslavska, I.; Thormann, W. *J. Chromatogr.* **1992**, *594*, 361.
(42) Kuhn, R.; Hoffstetter-Kuhn, S.; Wagner, H. *Electrophoresis* **1990**, *11*, 942.
(43) DeCuyper, M.; Joniau, M.; Dangreau, H. *Biochemistry* **1983**, *22*, 415.
(44) Kessler, R.; Manz, H.-J. *Electrophoresis* **1990**, *11*, 979.
(45) Graham, J. M.; Wilson, R. B. J.; Patel, K. *Methodol. Surv. Biochem. Anal.* **1987**, *17*, 143.
(46) Heidrich, H. G.; Hannig, K. *Methods Enzymol.* **1989**, *171*, 513.
(47) Hannig, K. *Electrophoresis* **1982**, *3*, 235.
(48) Roman, M. C.; Brown, P. R. *Anal. Chem.* **1994**, *66*, 86A.
(49) Clifton, M. J.; Jouve, N.; De Balmann, H.; Sanchez, V. *Electrophoresis* **1990**, *11*, 913.
(50) Hoffmann, P.; Wagner, H.; Weber, G.; Lanz, M.; Caslavska, J.; Thormann, W. *Anal. Chem.* **1999**, *71*, 1840.
(51) Raymond, D. E.; Manz, A.; Widmer, H. M. *Anal. Chem.* **1994**, *66*, 2858.
(52) Raymond, D. E.; Manz, A.; Widmer, H. M. *Anal. Chem.* **1996**, *68*, 2515.
(53) Hannig, K.; Wirth, H.; Schindler, R. K.; Spiegel, K. *Physiol. Chem.* **1977**, *358S*, 753.

(54) Kohlheyer, D.; Besselink, G. A. J.; Schlautmann, S.; Schasfoort, R. B. M. *Lab Chip* **2006**, *6*, 374.
(55) Kohlheyer, D.; Eijkel, J. C. T.; Schlautmann, S.; van den Berg, A.; Schasfoort, R. B. M. *Anal. Chem.* **2007**, *79*, 8190.
(56) Kohlheyer, D.; Eijkel, J. C. T.; Schlautmann, S.; van den Berg, A.; Schasfoort, R. B. M. *Anal. Chem.* **2008**, 4111.
(57) Fonslow, B. R.; Barocas, V. H.; Bowser, M. T. *Anal. Chem.* **2006**, *78*, 5369.
(58) Fonslow, B. R.; Bowser, M. T. *Anal. Chem.* **2005**, *77*, 5706.
(59) Fonslow, B. R.; Bowser, M. T. *Anal. Chem.* **2008**, *80*, 3182.
(60) Ding, H.; Li, X.; Lu, X.; Xu, J.; Sun, X.; Zhang, Z.; Wang, H.; Deng, Y. *Analyst* **2012**, *137*, 4482.
(61) Xu, Y.; Zhang, C.-X.; Janasek, D.; Manz, A. *Lab on a Chip* **2003**, *3*, 224.
(62) Zhang, C.-X.; Manz, A. *Anal. Chem.* **2003**, *75*, 5759.
(63) Albrecht, J. W.; El-Ali, J.; Jensen, K. F. *Anal. Chem.* **2007**, *79*, 9364.
(64) Albrecht, J. W.; Jensen, K. F. *Electrophoresis* **2006**, *27*, 4960.
(65) Mazereeuw, M.; de Best, C. M.; Tjaden, U. R.; Irth, H.; van der Greef, J. *Anal. Chem.* **2000**, *72*, 3881.
(66) Macounova, K.; Cabrera, C. R.; Holl, M. R.; Yager, P. *Anal. Chem.* **2000**, *72*, 3745.
(67) Fonslow, B. R.; Bowser, M. T. *Anal. Chem.* **2006**, *78*, 8236.
(68) Gebauer, P.; Bocek, P. *Anal. Chem.* **1997**, *69*, 1557.
(69) Bouskova, E.; Presutti, C.; Gebauer, P.; Fanali, S.; Beckers, J. L.; Bocek, P. *Electrophoresis* **2004**, *25*, 355.
(70) Weinberger, R. *Practical Capillary Electrophoresis, 2nd ed.*; Academic Press: San Diego, 2000.
(71) Mikkers, F. E. P.; Everaerts, F. M.; Verheggen, P. E. M. *J. Chromatogr.* **1979**, *169*, 1.
(72) Mikkers, F. E. P. *Anal. Chem.* **1999**, *71*, 522.
(73) Erny, G. L.; al., e. *Anal. Chem.* **2003**, *75*, 5197.
(74) Turgeon, R. T.; Bowser, M. T. *Electrophoresis* **2009**, *30*, 1342.
(75) Frost, N. W.; Bowser, M. T. *Lab Chip* **2010**, *10*, 1231.
(76) Lai, C. C. J.; Chen, C. H.; Ko, F. H. J. *J. Chromatogr. A* **2004**, *1023*, 143.
(77) Lacher, N. A.; Lunte, S. M.; Martin, R. S. *Anal. Chem.* **2004**, *76*, 2482.
(78) Abad-Villar, E. M.; Kuban, P.; Hauser, P. C. *Electrophoresis* **2005**, *26*, 3609.
(79) Kuban, P.; Hauser, P. C. *Electrophoresis* **2005**, *26*, 3169.
(80) Forry, S. P.; Murray, J. R.; Heien, M. L. A. V.; Locascio, L. E.; Wightman, R. M. *Anal. Chem.* **2004**, *76*, 4945.
(81) Herzig-Marx, R.; Quenney, K. T.; Jackman, R. J.; Schmidt, M. A.; Jensen, K. F. *Anal. Chem.* **2004**, *76*, 6476.
(82) Docherty, F. T.; Monaghan, P. B.; Keir, R.; Graham, D.; Smith, W. E.; Cooper, J. M. *Chem. Commun.* **2004**, 118.

(83) Park, T.; Lee, S.; Seong, G. H.; Choo, J.; Lee, E. K.; Kim, Y. S.; Ji, W. H.; Hwang, S. Y.; Gweon, D. G.; Lee, S. *Lab Chip* **2005**, *5*, 437.
(84) McDonnell, E. E.; Han, S.; Hilty, C.; Pierce, K. L.; Pines, A. *Anal. Chem.* **2005**, *77*, 8109.
(85) Ahola, S.; Casanova, F.; Perlo, J.; Munnemann, K.; Blumich, B.; Stapf, S. *Lab Chip* **2006**, *6*, 90.
(86) Dittrich, P. S.; Tachikawa, K.; Manz, A. *Anal. Chem.* **2006**, *78*, 3887.
(87) Nyholm, L. *Analyst* **2005**, *130*, 599.
(88) Macounova, K.; Cabrera, C. R.; Yager, P. *Anal. Chem.* **2001**, *73*, 1627.
(89) Lu, H.; Gaudet, S.; Schmidt, M. A.; Jensen, K. F. *Anal. Chem.* **2004**, *76*, 5705.
(90) de Jesus, D. P.; Blanes, L.; do Lago, C. L. *Electrophoresis* **2006**, *27*, 4935.
(91) Kobayashi, H.; Shimamura, K.; Akaida, T.; Sakano, K.; Tajima, N.; Funazaki, J.; Suzuki, H.; Shinohara, E. *J. Chromatogr. A* **2003**, *990*, 169.
(92) van Heeren, H. *Lab Chip* **2012**, *12*, 1022.
(93) Bings, N. H.; Wang, C.; Skinner, C. D.; Colyer, C. L.; Thibault, P.; Harrison, D. J. *Anal. Chem.* **1999**, *71*, 3292.
(94) Regnier, F. E.; Amini, A.; Chakraborty, A.; Geng, M.; Ji, J.; Riggs, L.; Sioma, C.; Wang, S.; Zhang, X. *LC GC N. Amer.* **2001**, *19*, 200.
(95) Oliver, S. G.; al., e. *Trends Biotechnol.* **1998**, *16*, 373.
(96) Southam, A. D.; Payne, T. G.; Cooper, H. J.; Arvanitis, T. N.; Viant, M. R. *Anal. Chem.* **2007**, *79*, 4595.
(97) Martin, M.; Herman, D. P.; Guiochon, G. *Anal. Chem.* **1986**, *58*, 2200.
(98) Wang, X.; Barber, W. E.; Carr, P. W. *J. Chromatogr. A* **2006**, *1107*, 139.
(99) Shen, Y.; Zhang, R.; Moore, R. J.; Kim, J.; Metz, T. O.; Hixson, K. K.; Zhao, R.; Livesay, E. R.; Udseth, H. R.; Smith, R. D. *Anal. Chem.* **2005**, *77*, 3090.
(100) Busnel, J.; Lion, N.; Girault, H. H. *Anal. Chem.* **2007**, *79*.
(101) Giddings, J. C. *Anal. Chem.* **1984**, *56*, 1258A.
(102) Karger, B. L.; Snyder, L. R.; Horvath, C. *An Introduction to Separation Science*; Wiley and Sons: New York, 1973.
(103) Guiochon, G.; Beaver, L. A.; Gonnord, M. F.; Siouffi, A. M.; Zakaria, M. *J. Chromatogr.* **1983**, *255*, 415.
(104) Rutan, S. C.; Davis, J. M.; Carr, P. W. *J. Chromatogr. A* **2012**, *1255*, 267.
(105) Dugo, P.; Cacciola, F.; Kumm, T.; Dugo, G.; Mondello, L. *J. Chromatogr. A* **2008**, *1184*, 353.
(106) Gilar, M.; Fridrich, J.; Schure, M. R.; Jaworski, A. *Anal. Chem.* **2012**, *84*, 8722.
(107) Murphy, R. E.; Schure, M. R.; Foley, J. P. *Anal. Chem.* **1998**, *70*, 1585.
(108) Davis, J. M.; Stoll, D. R.; Carr, P. W. *Anal. Chem.* **2007**, *80*, 461.
(109) Link, A. J.; Eng, J.; Schieltz, D. M.; Carmack, E.; Mize, G. J.; Morris, D. R.; Garvik, B. M.; Yates III, J. R. *Nat. Biotechnol.* **1999**, *17*, 676.

(110) Washburn, M. P.; Ulaszek, R.; Deciu, C.; Schieltz, D. M.; Yates III, J. R. *Anal. Chem.* **2002**, *74*, 1650.
(111) Washburn, M. P.; Wolters, D. A.; Yates III, J. R. *Nat. Biotechnol.* **2001**, *19*, 242.
(112) Wolters, D. A.; Washburn, M. P.; Yates III, J. R. *Anal. Chem.* **2001**, *73*, 5683.
(113) Wu, C. C.; MacCoss, M. J.; Howell, K. E.; Yates III, J. R. *Nat. Biotechnol.* **2003**, *21*, 532.
(114) Ramsey, J. D.; Jacobson, S. C.; Culbertson, C. T.; Ramsey, J. M. *Anal. Chem.* **2003**, *75*, 3758.
(115) Rocklin, R. D.; Ramsey, R. S.; Ramsey, J. M. *Anal. Chem.* **2000**, *72*, 5244.
(116) Shadpour, H.; Soper, S. A. *Anal. Chem.* **2006**, *78*, 3519.
(117) Osiri, J. K.; Shadpour, H.; Park, S.; Snowden, B. C.; Chen, Z. Y.; Soper, S. A. *Electrophoresis* **2008**, *29*, 4984.
(118) Cong, Y.; Zhang, L.; Tao, D.; Liang, Y.; Zhang, W.; Zhang, Y. *J. Sep. Sci.* **2008**, *31*, 588.
(119) Chambers, A. G.; Mellors, J. S.; Henley, W. H.; Ramsey, J. M. *Anal. Chem.* **2011**, *83*, 842.
(120) Mellors, J. S.; Black, W. A.; Chambers, A. G.; Starkey, J. A.; Lacher, N. A.; Ramsey, J. M. *Anal. Chem.* **2013**, *85*, 4100.
(121) Potts, L. W.; Stoll, D. R.; Li, X.; Carr, P. W. *J. Chromatogr. A* **2010**, *1217*, 5700.
(122) Turgeon, R. T.; Bowser, M. T. *Anal. and Bioanal. Chem.* **2009**, *394*, 187.
(123) Kostal, V.; Fonslow, B. R.; Arriaga, E. A.; Bowser, M. T. *Anal. Chem.* **2009**, *81*, 9267.
(124) Song, Y. A.; Hsu, S.; Stevens, A. L.; Han, J. *Anal. Chem.* **2006**, *78*, 3528.
(125) Jing, M.; Bowser, M. T. *Lab Chip* **2011**, *11*, 3703.
(126) Turgeon, R. T.; Fonslow, B. R.; Jing, M.; Bowser, M. T. *Anal. Chem.* **2010**, *82*, 3636.
(127) Zeiller, K.; Loeser, R.; Pascher, G.; Hannig, K. *Hoppe-Seyler's Z. Physiol. Chem.* **1975**, *356*, 1225.
(128) De Cuyper, M.; Joniau, M.; Dangreau, H. *Biochem. Biophys. Res. Commun.* **1980**, *95*, 1224.
(129) Nath, S.; Schuette, H.; Weber, G.; Hustedt, H.; Deckwer, W. D. *Electrophoresis* **1990**, *11*, 937.
(130) Poggel, M.; Melin, T. *Electrophoresis* **2001**, *22*, 1008.
(131) Zischka, H.; Weber, G.; Weber, P. J. A.; Posch, A.; Braun, R. J.; Buehringer, D.; Schneider, U.; Nissum, M.; Meitinger, T.; Ueffing, M.; Eckerskorn, C. *Proteomics* **2003**, *3*, 906.
(132) Zuo, X.; Lee, K.; Speicher, D. W. *Proteome Analysis* **2004**, 93.
(133) Wang, Y.; Hancock, W. S.; Weber, G.; Eckerskorn, C.; Palmer-Toy, D. *J. Chromatogr. A* **2004**, *1053*, 269.
(134) Brandon, N. P.; Kelsall, G. H. *J. Appl. Electrochem.* **1985**, *15*, 475.

(135) Blandamer, M. J.; Franks, F.; Haywood, K. H.; Tory, A. C. *Nature* **1967**, *216*, 783.
(136) Venczel, J. *Electrochim. Acta* **1970**, *15*, 1909.
(137) Giribabu, K.; Ghosh, P. *Chem. Eng. Sci.* **2007**, *62*, 3057.
(138) Jamialahmadi, M.; Mueller-Steinhagen, H. *Chem. Eng. J.* **1992**, *50*, 47.
(139) Shackman, J. G.; Watson, C. J.; Kennedy, R. T. *J. Chromatogr. A* **2004**, *1040*, 273.
(140) Helenius, A.; Simons, K. *Biochim. Biophys. Acta* **1975**, *415*, 29.
(141) Goheen, S. C.; Matsor, R. S. *J. Amer. Oil Chem. Soc.* **1989**, *66*, 994.
(142) *Surfactants*; Tadros, T. F., Ed.; Academic Press: London, 1984.
(143) Jańczuk, B.; Bruque, J. M.; González-Martín, M. L.; Dorado-Calasanz, C. *Langmuir* **1995**, *11*, 4515.
(144) Tartar, H. V. *J. Colloid Sci.* **1959**, *14*, 115.
(145) Oko, U. N.; Venable, R. L. *J. Colloid Interface Sci.* **1971**, *35*, 53.
(146) Lunkenheimer, K.; Czichocki, G.; Hirte, R.; Barzyk, W. *Colloids and Surfaces A: Physiochemical and Engineering Aspects* **1995**, *101*, 187.
(147) Zdziennicka, A. *Journal of Colloid and Interface Science* **2009**, *335*, 175.
(148) Surampudi, S.; Narayanan, S. R.; Vamos, E.; Frank, H.; Halpert, G.; LaConti, A.; Kosek, J.; Surya Prakash, G. K.; Olah, G. H. *Journal of Power Sources* **1994**, *47*, 377.
(149) Geiger, M.; Frost, N. W.; Bowser, M. T. *Anal. Chem.* **2014**, *Submitted*.
(150) Bien, D. C. S.; Rainey, P. V.; Mitchell, S. J. N.; Gamble, H. S. *J. Micromech. Microeng.* **2003**, *13*, S34.
(151) Grosse, A.; Grewe, M.; Fouckhardt, H. *J. Micromech. Microeng.* **2001**, *11*, 257.
(152) Bu, M. Q.; Melvin, T.; Ensell, G. J.; Wilkinson, J. S.; Evans, A. G. R. *Sens. Actuator A-Phys.* **2004**, *115*, 476.
(153) Tay, F. E. H.; Iliescu, C.; Jing, J.; Miao, J. M. *Microsystem Technologies* **2006**, *12*, 935.
(154) Iliescu, C.; Miao, J. M.; Tay, F. E. H. *Sens. Actuator A-Phys.* **2005**, *117*, 286.
(155) Ceyssens, F.; Puers, R. *J. Micromech. Microeng.* **2009**, *19*, 067001.
(156) Iliescu, C.; Jing, J.; Tay, F. E. H.; Miao, J. M.; Sun, T. T. *Surf. Coat. Technol.* **2005**, *198*, 314.
(157) Iliescu, C.; Miao, J. M.; Tay, F. E. H. *Surf. Coat. Technol.* **2005**, *192*, 43.
(158) Gretillat, M. A.; Paoletti, F.; Thiebaud, P.; Roth, S.; KoudelkaHep, M.; deRooij, N. F. *Sens. Actuator A-Phys.* **1997**, *60*, 219.
(159) Blas, M.; Delaunay, N.; Rocca, J. *Electrophoresis* **2008**, *29*, 20.
(160) Saito, R. M.; Coltro, W. K. T.; de Jesus, D. P. *Electrophoresis* **2012**, *33*, 2614.
(161) Jacobson, S. C.; Hergenroder, R.; Koutny, L. B.; Warmack, R. J.; Ramsey, J. M. *Anal. Chem.* **1994**, *66*, 1107.

(162) Jacobson, S. C.; Hergenroder, R.; Koutny, L. B.; Ramsey, J. M. *Anal. Chem.* **1994**, *66*, 1114.
(163) Jacobson, S. C.; Koutny, L. B.; Hergenroder, R.; Moore, A. W.; Ramsey, J. M. *Anal. Chem.* **1994**, *66*, 3472.
(164) Jacobson, S. C.; Hergenroder, R.; Moore, A. W.; Ramsey, J. M. *Anal. Chem.* **1994**, *66*, 4127.
(165) Harrison, D. J.; Fan, Z. H.; Seiler, K.; Manz, A.; Widmer, H. M. *Anal. Chim. Acta* **1993**, *283*, 361.
(166) Seiler, K.; Harrison, D. J.; Manz, A. *Anal. Chem.* **1993**, *65*, 1481.
(167) Zhang, C. X.; Manz, A. *Anal. Chem.* **2001**, *73*, 2656.
(168) Fluri, K.; Fitzpatrick, G.; Chiem, N.; Harrison, D. J. *Anal. Chem.* **1996**, *68*, 4285.
(169) Fu, L. M.; Lin, C. H. *Electrophoresis* **2004**, *25*, 3652.
(170) Shultz-Lockyear, L. L.; Colyer, C. L.; Fan, Z. H.; Roy, K. I.; Harrison, D. J. *Electrophoresis* **1999**, *20*, 529.
(171) Fu, L. M.; Yang, R. J.; Lee, G. B.; Pan, Y. J. *Electrophoresis* **2003**, *24*, 3026.
(172) Moring, S. E.; Colburn, J. C.; Grossman, P. D.; Lauer, H. H. *LC GC-Mag. Sep. Sci.* **1990**, *8*, 34.
(173) Gendron, P. O.; Avaltroni, F.; Wilkinson, K. J. *J. Fluoresc.* **2008**, *18*, 1093.
(174) Dutta, P.; Beskok, A. *Anal. Chem.* **2001**, *73*, 1979.
(175) Zholkovskij, E. K.; Masliyah, J. H. *Anal. Chem.* **2004**, *76*, 2708.
(176) Kraly, J. R.; Jones, M. R.; Gomez, D. G.; Dickerson, J. A.; Harwood, M. M.; Eggertson, M.; Paulson, T. G.; Sanchez, C. A.; Odze, R.; Feng, Z. D.; Reid, B. J.; Dovichi, N. J. *Analytical Chemistry* **2006**, *78*, 5977.